POLITECNICO DI TORINO
Repository ISTITUZIONALE

Study of the interaction between baryons and light mesons via femtoscopy at the LHC

Original
Study of the interaction between baryons and light mesons via femtoscopy at the LHC / Abualrob, I.J., Acharya, S., Aglieri Rinella, G., Aglietta, L., Agrawal, N., Ahammed, Z., Ahmad, S., Ahuja, I., Akbar, Z.U.L., Akindinov, A., Akishina, V., Al-Turany, M., Aleksandrov, D., Alessandro, B., Alfaro Molina, R., Ali, B., Alici, A., Alkin, A., Alme, J., Alocco, G., et al.. - In: PHYSICS LETTERS. SECTION B. - ISSN 0370-2693. - 874:(2026). [10.1016/j.physletb.2026.140227]

Availability:
This version is available at: 11583/3016098 since: 2026-09-29T20:20:30Z

Publisher:
Elsevier

Published
DOI:10.1016/j.physletb.2026.140227

Terms of use:

This article is made available under terms and conditions as specified in the corresponding bibliographic description in the repository

Publisher copyright

(Article begins on next page)

25 October 2026

Phys. Lett. B 874 (2026) 140227

Contents lists available at ScienceDirect

Physics Letters B

journal homepage: www.elsevier.com/locate/physletb

Letter

Study of the interaction between Ξ baryons and light mesons via femtoscopy at the LHC

ALICE Collaboration [1]

ARTICLE INFO

Editor: Dr. M. Doser

Keywords:
Meson-baryon interaction
Strong interaction
Femtoscopy
Strangeness
Molecular states

ABSTRACT

Meson-baryon systems with strangeness content provide a unique laboratory for investigating the strong interaction and testing theoretical models of hadron structure and dynamics. In this work, the measured correlation functions for oppositely charged Ξ-K and $\Xi-\pi$ pairs obtained in high-multiplicity pp collisions at $\sqrt{s} = 13$ TeV at the LHC are presented. For the first time, high-precision data on the Ξ-K interaction are delivered at small relative momenta. The scattering lengths, extracted via the Lednický–Lyuboshits expression of the pair wavefunction, indicate a repulsive and a shallow attractive strong interaction for the Ξ-K and $\Xi-\pi$ systems, respectively. The Ξ(1620) and Ξ(1690) states are observed in the $\Xi-\pi$ correlation function and their properties, mass and width, are determined. These measurements are in agreement with other available results. Such high-precision data can help refine the understanding of these resonant states, provide stronger constraints for chirally motivated potentials, and address the key challenge of describing the coupled-channel dynamics that may give rise to molecular configurations .

1. Introduction

Understanding the strong force acting at the hadronic level is fundamental for the development of Quantum Chromodynamics (QCD) in the non-perturbative regime. The experimental and theoretical efforts in the study of the hadron spectrum over several decades revealed features of QCD which lead to the appearance of exotic states beyond the conventional classification of hadrons with two and three valence quarks (mesons and baryons). This scenario is particularly evident for the charm sector, with several observations of tetra- and penta-quark states at high-energy pp and e^+e^- collider experiments [1,2]. In the light sector, where u, d and s quarks are considered, several predictions for molecular states exist, in particular for the meson-baryon sectors with strangeness $S = -1$ [3–9] and $S = -2$ [10–14]. The origin of these hadronic molecules lies in the characteristic coupled-channel dynamics occurring among meson-baryon pairs sharing the same quantum numbers. This coupled-channel interplay enables at the level of the interaction possible transitions, occurring both on- and off-shell, from one channel to the other. An example of a molecular state, the only one widely accepted so far, is the Λ(1405), whose double-pole structure has been assessed to be arising from the $\pi\Sigma - \overline{K}N$ coupling [3]. A stranger counterpart of the Λ(1405) is represented by the Ξ(1620) in the $S = -2$ meson-baryon sector, whose structure is still rather unclear. This state was observed for the first time in 2019 by the Belle collaboration in the $\Xi-\pi$ channel [12]. Along with the Ξ(1620), also the Ξ(1690) can be interpreted as a molecular state due to its proximity to the $\Sigma\overline{K}$ channels [11,13]. Thanks to a larger amount of spectroscopy data, in both Λ–K^- [15] and $\Xi-\pi$ [12] final states, the properties of this state, such as mass and width, are better known.

Effective field theories (EFTs), such as Chiral Perturbation Theory (ChPT) [16,17], offer a systematic framework to investigate the nature and composition of these challenging states. They enable the inclusion of higher-order corrections in the interaction terms and make it possible to predict physical properties such as masses, decay widths, and scattering amplitudes. Both the Ξ(1620) and Ξ(1690) states have been investigated within perturbation theories based on chirally-motivated Lagrangians, starting from the first Ξ(1620) prediction in Ref. [10], followed by a subsequent work in Ref. [18], in which a second pole was found and assigned to the Ξ(1690). EFT-based potentials involving elastic and inelastic transitions depend on the so-called low energy constants [19], which must be determined from fits to the data. The number of these parameters increases as the potentials are extended to higher orders, hence larger data sets in wide energy ranges are needed as input, in particular for recent calculations at next-to-leading order (NLO) [20]. In the strangeness sector, such experimental inputs are often scarce and challenging to obtain, due to the difficulties in performing experiments with unstable strange particles.

Femtoscopy applied in high-energy pp and nucleus-nucleus collisions has been proved to be a powerful experimental technique, able to provide precise data on hadron-hadron interactions [21,22]. Studies on the

Contact: ALICE Publications (alice-publications@cern.ch).
[1] See Appendix B for the list of collaboration members

https://doi.org/10.1016/j.physletb.2026.140227
Received 8 October 2025; Received in revised form 27 December 2025; Accepted 28 January 2026
Available online 2 February 2026
0370-2693/© CERN for the benefit of the ALICE Collaboration. Published by Elsevier B.V. Funded by SCOAP³. This is an open access article under the CC BY license (http://creativecommons.org/licenses/by/4.0/).

S = −2 meson-baryon interaction via measurements of Λ–$\overline{K}$ correlations in pp [23] and Pb–Pb [24] systems delivered for the first time evidence of the Ξ(1620) at the Λ–K$^-$ channel threshold, offering a complementary approach to spectroscopy for investigating these molecular states by unveiling the interaction between their constituents [13]. A further improvement in NLO Lagrangians, aimed at describing the S = −2 meson-baryon interaction and the nature of molecular candidates in this sector, requires precise experimental input on the $\Xi - \pi$ system [11,14], which is dynamically coupled to Λ–$\overline{K}$ and provides crucial constraints on the coupled-channel dynamics.

The S = −1 meson-baryon interaction is constrained by low-energy $\overline{K}$N scattering [25–30] and kaonic atom data [31], but theoretical models often exhibit discrepancies not only in describing the Λ(1405) region below the $\overline{K}$N threshold but also at significantly higher energies. ALICE used femtoscopy as an alternative method to study the $\overline{K}$N threshold interaction via K$^-$p [32–34] correlations across pp, p–Pb and Pb–Pb collisions. The femtoscopy measurements of K$^-$p pairs, in particular in small collision systems, demonstrated high sensitivity to the interplay among the different channels in this sector. The region of energy well above the $\overline{K}$N threshold is more challenging to be explored experimentally since it involves systems with a neutral meson (η) and a multi-strange baryon (Ξ), which are difficult to reconstruct due to low detection efficiency or low production yield. Inelastic cross sections of K$^-$p → ηΛ, ηΣ^0, K$^0\Xi^0$ and K$^+\Xi^-$ reactions are available, but are subject to large uncertainties, which impede the extraction of precise information on the underlying interaction [27,29,35–46]. Dedicated studies based on ChPT calculations at NLO showed how incorporating data from high-energy channels leads to tighter constraints on the model [20,47–49]. The Ξ-K channel is of particular relevance since it allows to investigate the isospin-triplet component of the S = −1 meson-baryon interaction [50], currently poorly constrained due to the limited availability of scattering data. Precise data on the Ξ-K interaction [51], in particular using femtoscopy [52], are able to provide crucial experimental input for model discrimination across a wide energy range.

This work presents the first measurement of femtoscopic correlations between Ξ^- baryons (dss) and K$^+$ (u$\overline{s}$) and π^+ (u$\overline{d}$) mesons, and charge conjugates, in high-multiplicity (HM) ppcollisions at $\sqrt{s}$ = 13 TeV, recorded by ALICE at the Large Hadron Collider. The obtained correlations are compared with available models and the scattering parameters for the Ξ-K and $\Xi - \pi$ interaction are extracted through a fit using the Lednický–Lyuboshits wavefunction including both the strong and Coulomb interactions. In the fit to the $\Xi - \pi$ correlation function, the properties of Ξ(1620) and Ξ(1690) states are determined.

2. Data analysis

A total of 1×10^9 high-multiplicity pp collisions at $\sqrt{s} = 13$ TeV were selected by ALICE [53] using an online trigger based on the total signal amplitude measured by the V0 detector [54], which consists of two plastic scintillator arrays located on both sides of the collision point along the beam axis. The selected HM events correspond to the 0.17% highest-multiplicity events in the sample of inelastic collisions with at least one measured charged particle within the pseudorapidity range $|\eta| < 1$ (INEL > 0). The primary interaction vertex is reconstructed by extrapolating track segments from the innermost layers of the Inner Tracking System (ITS) [55], composed of six layers of silicon detectors providing high-precision position measurements, back to the beam line. Events with multiple reconstructed vertices are efficiently identified as in-bunch pile-up and rejected from the analysis [56]; in the HM sample, the residual pile-up contamination is at the percent level and has a negligible impact on the final results. These HM events have an average charged-particle multiplicity density at midrapidity ($|\eta| < 0.5$) of $\langle dN_{ch}/d\eta \rangle \approx 30$, about 4 times larger than the INEL > 0 events. It is also worth noting the enhanced production of hyperons in HM events [57] which facilitates the collection of large samples of the particle pairs of interest for this analysis.

Charged particles are reconstructed and identified using the ITS, the Time Projection Chamber (TPC) [58], and the Time Of Flight detector (TOF) [59], which are immersed in a uniform magnetic field of 0.5 T along the beam direction and cover the pseudorapidity range $|\eta| < 0.9$. The TPC is a cylindrical gaseous detector that performs particle tracking and identification by measuring the specific energy loss (dE/dx). The TOF detector consists of Multigap Resistive Plate Chambers and provides timing information. Charged particles used for this analysis, including decay products from reconstructed Ξ decays, are required to be within the pseudorapidity range $|\eta| < 0.8$. The transverse-momentum (p_T) resolution for charged particles typically varies from about 2 % for tracks with $p_T = 10$ GeV/c to below 1 % for $0.14 < p_T < 1$ GeV/c.

Pions (kaons) are selected with a minimum transverse momentum of 0.14 (0.20) GeV/c. Particle identification (PID) is performed using the dE/dx measurement in the TPC and the timing information from the TOF, both as a function of the reconstructed track momentum. The basic selection criteria for charged particles can be found in Ref. [60], and further details on the pion (kaon) selection are given in Refs. [61–63]. The purity of the pion and kaon sample was estimated to be 98% and 100%, respectively, using Monte Carlo (MC) simulations. The primary fraction, i.e. the fraction of particles stemming directly from the collision point, is calculated using the Monte Carlo template procedure described in Ref. [64] and it amounted to 94% for pions and 99% for kaons.

The identification of charged Ξ baryons exploits their characteristic weak decay cascade pattern. The primary decay is $\Xi^- \to \Lambda + \pi^-$, which has a branching ratio (BR) of nearly 100% [65]. This is subsequently followed by the weak decay of the daughter Λ baryon, Λ → p+π^- (BR = 63.9 ± 0.5% [65]) . The selection of Ξ candidates is performed in two main steps. First, a pre-selection step applies loose, single-variable requirements on several topological quantities, as well as on the invariant masses of the Λ and Ξ candidates. This initial stage is designed to minimize signal loss rather than aggressively reduce combinatorial background. In the second step, a multivariate analysis (MVA) is employed using a Boosted Decision Tree (BDT) technique, as detailed in Ref. [66]. A similar procedure was already used in previous femtoscopy analyses by ALICE involving D mesons [61,67]. A total of nine variables serve as input for the BDT. These include the distance of closest approach (DCA) between tracks, the DCA of tracks to the primary and decay vertices, the pointing angles of the Λ and Ξ candidates, and PID information for the charged particles. The BDT is trained using MC simulations for the signal, where the production and decay of Ξ baryons in HM pp events are simulated with PYTHIA. The reconstruction of Ξ candidates is performed after propagating the daughter tracks through a full detector simulation incorporating the ALICE geometry and response using GEANT3 [68]. The combinatorial background sample for the training is derived from data candidates that pass the pre-selection criteria but have a Ξ invariant mass outside the signal region, specifically within the ranges 1280–1308 MeV/c^2 and 1322–1370 MeV/c^2. The application of the BDT selection significantly enhances the purity of the Ξ sample while maintaining high signal efficiency. Following an optimization of the BDT output score threshold used to select signal candidates, the purity of the selected Ξ sample reaches 97%, with minimal signal loss relative to the pre-selected data. Finally, Ξ candidates are retained if their invariant mass falls within a 10 MeV/c^2 window centered around the nominal Ξ^- mass.

The relative momentum between the selected particles in their pair rest frame, denoted as k^*, is measured for all combinations of interest. The experimental correlation function is then determined as

$$C(k^*) = \mathcal{N} \frac{N_{\text{same}}(k^*)}{N_{\text{mixed}}(k^*)}, \tag{1}$$

where $N_{\text{same}}(k^*)$ represents the k^* distribution constructed from pairs of particles emitted within the same collision event. The $N_{\text{mixed}}(k^*)$ distribution, which serves as a reference for uncorrelated pairs, is obtained by pairing particles from different events that exhibit similar primary vertex z-positions and event multiplicities. To account for the differ-

ing event sample sizes, the mixed-event distribution is normalized, via the constant $\mathcal{N}$, to the same-event distribution within the range $k^* \in$ [1000–1200] MeV/c, a region of the spectra where final state interaction (FSI) and resonance effects are absent.

The correlation functions are calculated for all oppositely charged particle combinations. No statistically significant differences are observed between the correlation functions of Ξ^-–K^+ and $\overline{\Xi}^+$–K^- pairs, nor between Ξ^-–π^+ and $\overline{\Xi}^+$–π^- pairs. Since the correlation functions are expected to be identical for charge-conjugate pairs, the respective pairs are combined to improve statistical precision. In the following, Ξ-K and $\Xi-\pi$ refer to the correlation functions obtained from summing the distributions of pairs and theirs charge-conjugates.

In the case of $\Xi-\pi$ correlations, autocorrelation effects are mitigated by excluding pions identified as decay products of Ξ baryons from the pairing. Detector effects, such as track merging or track splitting, are evaluated by analyzing the $\Delta\eta-\Delta\varphi^*$ distributions, with φ^* being the azimuthal coordinate between the Ξ decay products and the paired meson at several radial positions within the TPC volume. These contributions are found to be negligible. Possible effects from combinatorial background due to out-of-bunch collision pile-up in the TPC are evaluated by repeating the analysis while requiring that all charged tracks have a matched hit in either the ITS or the TOF, which can provide precise timing information to remove pile-up contamination. The effect is found to be negligible, and therefore, this requirement is not applied in the final analysis.

The measured Ξ-K and $\Xi-\pi$ correlation functions are presented in Figs. 1 and 3, respectively. The corresponding figures with extended k^* range can be seen in the Appendix A. The systematic uncertainties of the data points, depicted as shaded boxes in the figures, are estimated by varying the track selection criteria, following the procedure used in previous ALICE femtoscopy analyses, see Refs. [63,69] for the procedure and for pion and kaon selections. For the Ξ selection, the BDT threshold is varied within 25%. The total systematic uncertainty remains below 1% for both measured correlation functions in all k^* bins. Both the Ξ-K and $\Xi-\pi$ correlation functions show a clear signal of the FSI in the low relative momentum region, visible as a deviation from unity. The Ξ-K correlation also shows a steadily increasing baseline, an enhancement that grows as k^* decreases that is clearly visible in the region above 200 MeV/c, where FSI effects are negligible. This behavior contrasts with the $\Xi-\pi$ data, which show no such trend and remain mostly constant in the large k^* region. Additionally, the $\Xi-\pi$ correlation shows a prominent peak at $k^* \approx 150$ MeV/c, corresponding to the invariant mass of $\approx$ 1530 MeV/c^2, where the signal of the Ξ(1530) decaying into the $\Xi-\pi$ pairs with BR of 100% [65] is expected, and other structures. The features shown by both correlation functions are discussed in Sections 3–5.

3. Analysis of the correlation function

The measured correlation functions for Ξ-K and $\Xi-\pi$ pairs are fitted using the expression

$$C_{\rm tot}(k^*) = N_{\rm D} \times C_{\rm model}(k^*) \times C_{\rm background}(k^*), \tag{2}$$

where $N_{\rm D}$ is a normalization constant, left free to vary in the fit. Due to the different contribution of the background in the two pairs, discussed in details later in this section, the total fit range is $k^* \in [0, 1000]$ MeV/c for $\Xi-\pi$ and $k^* \in [0, 1600]$ MeV/c for Ξ-K. The modeling term $C_{\rm model}(k^*)$ in Eq. (2) is analogous for both pairs and it is expressed as

$$C_{\rm model}(k^*) = \lambda_{\rm gen} C_{\rm gen}(k^*) + \lambda_{{\rm M-\Xi(1530)^{ch.}}} C_{{\rm M-\Xi(1530)^{ch.}}}(k^*) + \lambda_{\rm M-\tilde{\Xi}} C_{\rm M-\tilde{\Xi}}(k^*) + \lambda_{\rm flat} C_{\rm flat}. \tag{3}$$

Each of the contributions entering in the modeled correlation is weighted by a corresponding λ parameter, representing its relative fraction in the measured sample.

The first term $C_{\rm gen}(k^*)$ embeds the correlation signal stemming from the genuine FSI of meson-Ξ pairs. The corresponding $\lambda_{\rm gen}$ amounts to 0.68 and 0.61 for Ξ-K and $\Xi-\pi$ pairs, respectively, and is determined as a product of the purity and fractions of the considered particles [64], provided in Section 2.

The second term, $C_{{\rm M-\Xi(1530)^{ch.}}}(k^*)$, accounts for residual correlations arising when a primary pion/kaon (meson, M) is paired with a Ξ originating from the decay of a charged (ch.) Ξ(1530) resonance. A fraction of reconstructed Ξ candidates indeed stems from the strong decay $\Xi(1530)^{-,0} \to \Xi^-\pi^{0,+}$, leading to a residual correlation that dilutes the genuine signal in the correlation function. Since no theoretical predictions exist for the strong interaction between mesons and excited Ξ(1530) states, only the contribution from the charged $\Xi(1530)^-$ ($\bar{\Xi}(1530)^+$) is modeled, assuming Coulomb interaction via the CATS framework [70]. The relative k^* between the charged Ξ(1530) and the meson is transformed, via the decay kinematics, into that of the measured $\Xi-\pi$ and Ξ-K pairs. The corresponding weight $\lambda_{{\rm M-\Xi(1530)^{ch.}}} = 0.14$ is evaluated following the same approach of Ref. [71] and is based on the measurement of the $\Xi(1530)^0$ yield in pp collisions at 7 TeV [72]. In contrast, contributions from initial M-$\Xi(1530)^0$ pairs, with a relative contribution of 0.07, are assumed to be flat (equal to unity for any k^*) and are absorbed into the $\lambda_{\rm flat}$ term (see below).

The third term in Eq. (3), $C_{\rm M-\tilde{\Xi}}(k^*)$, includes the contribution from primary mesons paired to misidentified Ξ candidates and it amounts to $\lambda_{\rm M-\tilde{\Xi}} = 0.03$. This residual contribution is modeled in a data-driven approach by calculating the correlation function using a selection of misidentified Ξ candidates, realized by requiring a very low BDT score in the Ξ selection.

Finally, the last term in Eq. (3) refers to remaining contributions for which independence on k^* is assumed and hence $C_{\rm flat}$ is equal to unity, with a total weight $\lambda_{\rm flat} = 0.15$. The dominant contribution to $\lambda_{\rm flat}$ arises from Ξ(1530) feed-down. The remaining contributions consist of pairs where pions or kaons are misidentified and, for Ξ-K pairs, kaons originating from the decay of ϕ mesons. The latter contribution is calculated consistently with previous femtoscopic studies involving kaons [23,61].

To model the genuine $C_{\rm gen}(k^*)$ contribution, the Lednický–Lyuboshits (LL) wavefunction approach for a charged pair is employed, including both strong and Coulomb interactions in s-wave [73]. The corresponding relative wave function reads

$$\psi(\vec{k}^*, \vec{r}^*) = e^{i\delta_c}\sqrt{A_c(\eta)}\left[e^{-i\vec{k}^*\cdot\vec{r}^*}F(-i\eta, 1, i\xi) + f_C(k^*)\frac{\tilde{G}(\rho,\eta)}{r^*}\right]. \tag{4}$$

Here, $\eta = (k^* a_C)^{-1}$ with a_C being the Bohr radius and $\delta_c = \mathrm{Arg}[\Gamma(1 + i\eta)]$ is the s-wave Coulomb phase-shift. The variable $\xi = \rho(1 + \cos(\theta^*))$ is given in terms of $\rho = k^* r^*$, with r^* representing the distance between the emitted particles and θ^* being the angle between $\vec{k}^*$ and $\vec{r}^*$. The asterisk refers to the evaluation in the pair rest frame. The term $A_C(\eta) = 2\pi\eta\left[\exp(2\pi\eta) - 1\right]^{-1}$ represents the Coulomb penetration factor. The asymptotic expression of the Coulomb wave function is given by the term $e^{-i\vec{k}^*\cdot\vec{r}^*}F(\alpha, 1, z)$ together with $\widetilde{G}(\rho,\eta)$, where $F(\alpha, 1, z)$ is a confluent hypergeometric function and $\widetilde{G}(\rho,\eta) = \sqrt{Ac}(G_0 + iF_0)$ is a combination of the regular (F_0) and singular (G_0) s-wave Coulomb functions. The strong interaction is taken into account using the Coulomb-corrected scattering amplitude defined as

$$f_C(k^*) = \left[\frac{1}{f_0} + \frac{d_0 k^{*2}}{2} - ik^* A_C(k^*) - \frac{2}{a_C}h(k^*)\right]^{-1}, \tag{5}$$

with the effective range d_0 and the complex scattering length $f_0 = \Re f_0 + i \cdot \Im f_0$. Here, the real and imaginary part of f_0 take into account the elastic and inelastic part on the interacting potential, respectively. The last term depends on the function $h(k^*) = \frac{1}{(k^* a_C)^2}\sum_{n=1}^{\infty}\left[n\left(n^2 + (k^* a_C)^{-2}\right)\right]^{-1} - \gamma + \ln|k^* a_C|$ with the Euler constant γ equal to 0.5772. In order to leave only the real ($\Re f_0$) and imaginary ($\Im f_0$) parts of the scattering length f_0 as free parameters to be determined from a fit to the data, the calculation is performed assuming a zero effective range d_0. Note that there are known limitations of the LL model, particularly when dealing with the small source sizes character-

istic of pp collisions and in presence of a rich coupled-channel dynamics, as in the systems under study [63,70,74–77]. The LL approach has been employed in this study in order to provide an indication on the character and strength of strong interaction acting between Ξ baryons and the light mesons.

In order to calculate the modeled correlations via the Koonin–Pratt formula [78,79], information on the emitting source size and profile are needed. Following previous femtoscopic analyses performed in the same high-multiplicity data sample, the Resonance Source Model (RSM) [80,81] is employed. The RSM is based on a data-driven approach in which the source is composed by a Gaussian core, common to all pairs and dependent only on the pair transverse mass m_{T}, and a non-Gaussian tail due to strongly-decaying resonances. The transverse mass of the pair is defined here as $m_{\mathrm{T}} = \sqrt{k_{\mathrm{T}}^2 + m^2}$, with pair transverse momentum k_{T} and average pair mass m. Recent works on same-charge $\pi-\pi$ and p–π pairs performed by the ALICE collaboration confirmed the validity of this approach [62,69]. The core radius for Ξ-K pairs, determined following Ref. [81], is $r_{\mathrm{core}}(\langle m_{\mathrm{T}}\rangle = 1.69\ \mathrm{GeV}/c^2) = 0.89 \pm 0.04$ fm , and the one for $\Xi-\pi$ is $r_{\mathrm{core}}(\langle m_{\mathrm{T}}\rangle = 1.55\ \mathrm{GeV}/c^2) = 0.94 \pm 0.04$ fm. As observed already in previous femtoscopy studies [23,61], the presence of long-lived strong resonances decaying into kaons and pions introduces a significant exponential tail to the source profile for large r^*. Consequently, a simple Gaussian function fails to describe the full source profile. Following the approach used in the femtoscopy studies on $\Lambda\mathrm{K}^{\pm}$ in Ref. [23], the total core-halo source is therefore modeled with a weighted sum of two Gaussian functions, $S_1(r^*)$ and $S_2(r^*)$, weighted by the terms ω_{S} and λ_{S}, leading to an effective emitting source $S_{\mathrm{eff}}(r^*) = \lambda_{\mathrm{S}}[\omega_{\mathrm{S}} S_1(r^*) + (1-\omega_{\mathrm{S}})S_2(r^*)]$. The values of the source parametrization for Ξ-K ($\Xi-\pi$) pairs are $r_1 = 1.00 \pm 0.04$ fm, $r_2 = 2.45 \pm 0.04$ fm, $\lambda_{\mathrm{S}} = 0.97$, and $\omega_{\mathrm{S}} = 0.86$ ($r_1 = 1.19 \pm 0.04$ fm, $r_2 = 3.16 \pm 0.04$ fm, $\lambda_{\mathrm{S}} = 0.97$, and $\omega_{\mathrm{S}} = 0.74$).

A significant difference between the modeling of the Ξ-K, which occurs solely via Eq. (3), and the $\Xi-\pi$ pairs must be highlighted, and lies in the presence of several states in the latter. In particular, as can be seen in Fig. 3, the peak of the Ξ(1530) is observed at $k^* \approx 145$ MeV/c. Additionally, the Ξ(1620) and Ξ(1690), expected to appear at $k^* \approx 240$ MeV/c and at $k^* \approx 303$ MeV/c, can be identified. Both these states lie close to the opening of the $\Lambda\bar{\mathrm{K}}^0$ ($k^*_{\Lambda\bar{\mathrm{K}}^0} = 232$ MeV/c) and $\Sigma^0\bar{\mathrm{K}}^0 - \Sigma^{\pm}\mathrm{K}^{\mp}$ ($k^*_{\Sigma\bar{\mathrm{K}}} = 297-304$ MeV/c) channels coupled to the $\Xi-\pi$ system. The current data do not permit an unambiguous identification between the channel openings and the resonant structures in this momentum region. For the same reason, the $\Xi^0\eta$ opening and the Ξ(1950) state, at $k^* \approx 446$ MeV/c and $k^* \approx 513$ MeV/c respectively, cannot be discriminated from the combinatorial background. Since the two visible Ξ(1620) and Ξ(1690) states carry as well information on the underlying $\Xi-\pi$ interaction, the modeled correlation for the $\Xi-\pi$ system includes as well these contributions, namely in the form

$$C^{(\Xi-\pi)}_{\mathrm{model}}(k^*) = C_{\mathrm{model}}(k^*) + \sum_i w_i f_i(M_i, \Gamma_i), \tag{6}$$

where the sum i runs over the three Ξ^* states of mass M_i, width Γ_i, each described with a distribution f_i weighted by the parameters w_i to be determined in the fit. The narrow Ξ(1530) is modeled assuming a Voigt distribution with mass and width given by the PDG values [65]. The corresponding Gaussian broadening due to finite momentum resolution is also applied while performing the fit. The broader Ξ(1620) and Ξ(1690) states are modeled via a Breit-Wigner profile distribution with masses and widths extracted from the fit.

The final contribution needed to compare the total fit function in Eq. (2) with the measured correlations is the background $C_{\mathrm{background}}(k^*)$. As already observed in several meson-baryon pairs [23,32,33,61,82], the dominant contribution to the non-femtoscopic signal is coming from the so-called mini-jet background. This background is typically associated with the initial hard processes occurring at the partonic level during the ppcollision [83], which can produce correlations visible up to k^* values of around 1 GeV/c or more. The effect of this background on the measured correlation has been observed to increase when the net-quantum numbers (baryon B, charge Q, strangeness S) within the pair are conserved [84]. Such a trend has been observed for example in the measured $\Lambda\mathrm{K}^+$ (S = 0) and $\Lambda\mathrm{K}^-$ (S = −2) correlations in Ref. [23]. Therefore, a much larger contribution in the Ξ-K case, in which an $s\bar{s}$ pair is present in the final-state hadrons and can originate from a common partonic source, with respect to the $\Xi-\pi$ one is expected. For both pairs, the $C_{\mathrm{background}}(k^*)$ was built from Monte Carlo simulations based on the PYTHIA 8.2 generator [85] (Monash tune [86]), and a simulation of the ALICE detector using GEANT3 [68]. For the $\Xi-\pi$ system, the PYTHIA simulation provides a reasonable description of the data outside the femtoscopic region of $k^* \geq 200$ MeV/c. The MC correlation is hence fitted in this case with a third-order degree polynomial in the range $k^* \in [0, 1200]$ MeV/c and kept fixed in the fit of the experimental $\Xi-\pi$ correlation function.

As anticipated, the mini-jet background in the Ξ-K system has a larger influence on the shape of the correlation function. The PYTHIA simulation captures the shape of the background correlation as a function of k^*, but the strength of the correlation is underestimated as compared to data. Hence, in order to describe the data outside the femtoscopic region and extrapolate this baseline to the lower k^* region, the correlation obtained from PYTHIA must be scaled. For this, the Ξ-K background component is expressed as

$$C^{(\Xi-K)}_{\mathrm{background}}(k^*) = 1 + (C_{\mathrm{MC}}(k^*) - 1) \times S, \tag{7}$$

where $C_{\mathrm{MC}}(k^*)$ represents the PYTHIA correlation function and S is a scaling factor parameter to be determined by fitting the data. The PYTHIA correlation is modeled with a functional form including three Gaussian functions, with its parameters determined by a fit to the PYTHIA MC data in a large momentum range $k^* \in [0, 1600]$ MeV/c in order to constrain as much as possible the shape. The ALICE collaboration has reported substantial differences between PYTHIA tunes in the description of the angular correlations induced for Ξ-K pairs produced in pp collisions [87]. In the current study, the Ropes tune [88] was explored as an alternative to Monash; however, it did not lead to a substantial improvement in the overall description. The need to scale the correlation strength persists as a requirement to achieve a better fit to the data.

4. Results on Ξ-K correlations

The experimental correlation function for Ξ-K pairs is presented in Fig. 1. The correlation function is fitted to the model presented in Section 3 using the LL approach that incorporates the Coulomb interaction and a parametrization of the strong interaction based on the scattering parameters. The fit is performed in the range $k^* \in [0, 1600]$ MeV/c. The resulting model of the correlation function, according to Eq. (3), is shown as the pink band in Fig. 1. The free parameters in this fit are $\Re f_0$ and $\Im f_0$ of the s-wave scattering length that enter in the LL model calculation of the wave-function, along with the parameter S scaling the MC description of the mini-jet baseline contribution. The mini-jet background alone is shown in Fig. 1 by the gray band. The lower panel shows the difference between the data and the modeled correlation function as a function of k^*, expressed in units of standard deviations ($n\sigma$), obtained by dividing the difference $C_{\mathrm{data}} - C_{\mathrm{model}}$ by the statistical uncertainty of the data. See full fit range figure in the Appendix A .

The widths of the pink and gray bands reflect the systematic uncertainties propagated from the fit. These uncertainties arise from several variations considered in the fitting procedure, namely: i) variation of the upper limit of the fit range by ±100 MeV/c; ii) variation in the functional form used to model the mini-jet background as given by PYTHIA simulations, including just two Gaussian functions instead of three; iii) variations in the λ parameters according to the uncertainties associated with their determination, which are at the level of 3%; iv) variations in the effective source radius according to the errors reported in the previous section. The fit is repeated for all possible combinations of these

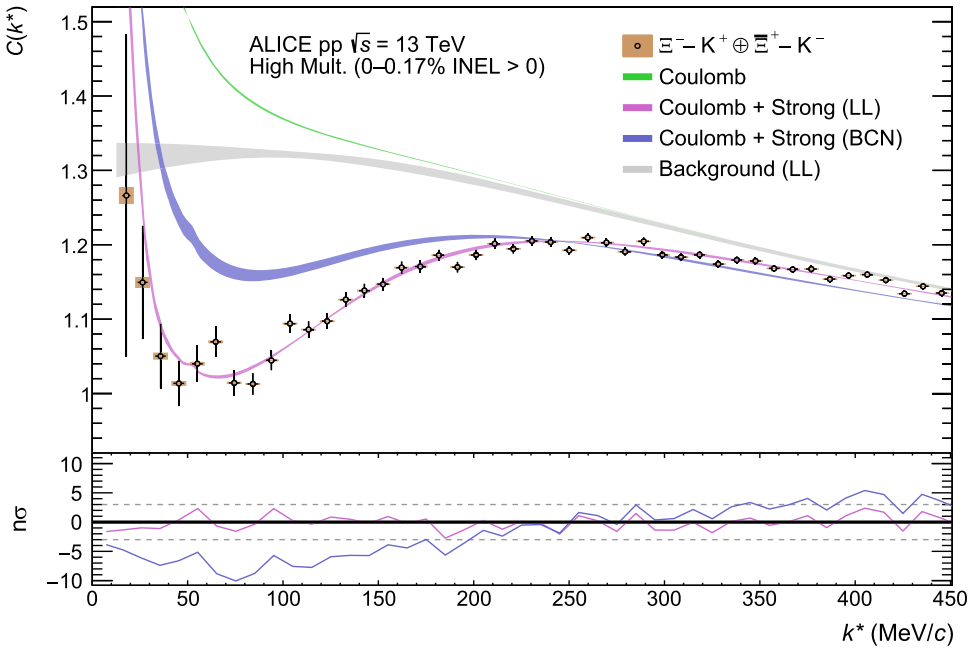

Fig. 1. Measured correlation function of Ξ-K pairs. Data are represented by the black circles, with statistical (black vertical lines) and systematic (orange boxes) uncertainties shown separately. The pink and blue bands represent the results from the fit considering strong and Coulomb FSI via the LL approach and the BCN model, respectively. The gray band represents the mini-jet background associated with the LL fit. The green line represents the Coulomb-only assumption. The lower panel presents the difference between the data and the modeled correlation functions for the LL (pink) and BCN (blue) models expressed as the number of standard deviations, nσ, see text for details.

variations. At each k^* value, the width of the band corresponds to one standard deviation of the resulting distribution of solutions.

Fig. 1 also displays the expectation from the Coulomb interaction alone, represented by the green line. To build the Coulomb-only correlation function, intended just as a qualitative test, the data have not been fitted again, instead the effect of the genuine FSI from the LL fit has been substituted by a Coulomb-only calculation, hence the mini-jet background baseline determined from the full LL fit is used. A clear difference is observed between the Coulomb-only expectation and the LL approach: the data lie significantly below the Coulomb-only curve, indicating that a repulsive strong interaction is necessary to describe the measured correlation function. Indeed the scattering parameters obtained from the LL fit are $\Re f_0 = -0.61 \pm 0.02(\text{stat.}) \pm 0.07(\text{syst.})$ fm and $\Im f_0 = 0.41 \pm 0.04(\text{stat.}) \pm 0.01(\text{syst.})$ fm . Such rather large value of the real part of the scattering length reflects the necessity of a sizable repulsive interaction, while the value of the imaginary part shows a large influence of the inelastic channels, as expected for the Ξ-K system, being the last channel opening in the S = −1 sector.

Furthermore, Fig. 1 includes a theoretical prediction from a unitarized ChPT (UChPT) approach in coupled-channels, the BCN model [52], shown as the blue line. This model derives unitarized s-wave meson-baryon scattering amplitudes from a chiral Lagrangian up to NLO. It is constrained to the available scattering data in the S = −1 sector, including the higher-energy $K^-p \to$ Ξ-K reactions, and it is capable of describing the K^-p correlation function measured by ALICE in pp collisions [32,33] and the signature from the channel coupling in such data. The BCN correlation function is calculated from these amplitudes using the Koonin–Pratt formula, applying the source function described in the previous section. The mini-jet background parameter S is also fitted when comparing the BCN model prediction to the data, although for clarity, the resulting baseline is not explicitly shown in the figure. The BCN model fails to describe the ALICE data in the low relative momentum region, showing a weaker anticorrelation than observed in the data. The scattering parameters for the Ξ-K interaction predicted by the BCN model, $\Re f_0 = -0.39$ fm, $\Im f_0 = 0.20$ fm, with an effective range of $d_0 = 0.668 + i \cdot (-0.683)$ fm, are indeed smaller in absolute value compared with the ones obtained using the LL model under the zero effective range approximation.

Another coupled-channel calculation, under the Dynamical Coupled-Channels (DCC) approach by the ANL-Osaka group [48,49], which also starts from SU(3) Lagrangians to derive meson-baryon potentials, also delivers scattering parameters that differ from those obtained from the LL fit to the data. The Ξ-K isospin averaged scattering lengths from the ANL-Osaka approach are obtained considering two different models, with $\Re f_0 = -0.76$ fm and $\Im f_0 = 0.11$ fm , and $\Re f_0 = -0.86$ fm and $\Im f_0 = 0.09$ fm. In this case the real part of the scattering length is larger than the results from the LL fit while the imaginary part is smaller. It is not surprising that the BCN and ANL-Osaka approaches deliver such different scattering parameters, even when both use the scattering data from reactions such as $K^-p \to$ Ξ-K as input in the high energy regime. The large uncertainties and limited availability of such data prevents from constraining the models at large energies [51] and this is reflected as well in the difficulties of describing the Ξ-K correlation data presented here.

Regarding a potential direct influence of resonant states on the Ξ-K correlation function, several theoretical frameworks predict indeed a plethora of Λ^* and Σ^* resonances that could couple to the Ξ-K channel across various energy ranges [47–49,89–92]. However, the statistical precision of the current ALICE Ξ-K femtoscopic data is insufficient to discern clear, statistically significant structures in the correlation function that could be unambiguously attributed to the decay of such resonances into Ξ-K. Consequently such resonant states are not considered in the fits to the experimental Ξ-K correlation function, although their undetected presence could influence the modeling of the measured correlations. Moreover, the possible presence of bound states or resonances below the Ξ-K threshold could induce an additional depletion of the correlation function. It is worth noting that the BCN model used for comparison with the data does not dynamically generate such states.

Fig. 2 shows a data-driven extracted genuine Ξ-K correlation function, obtained by identifying $C_{\text{tot}}(k^*)$ in Eq. (2) with the experimental Ξ-K correlation function and isolating the $C_{\text{gen}}(k^*)$ contribution in Eq. (3). The associated systematic uncertainties, depicted by the orange boxes,

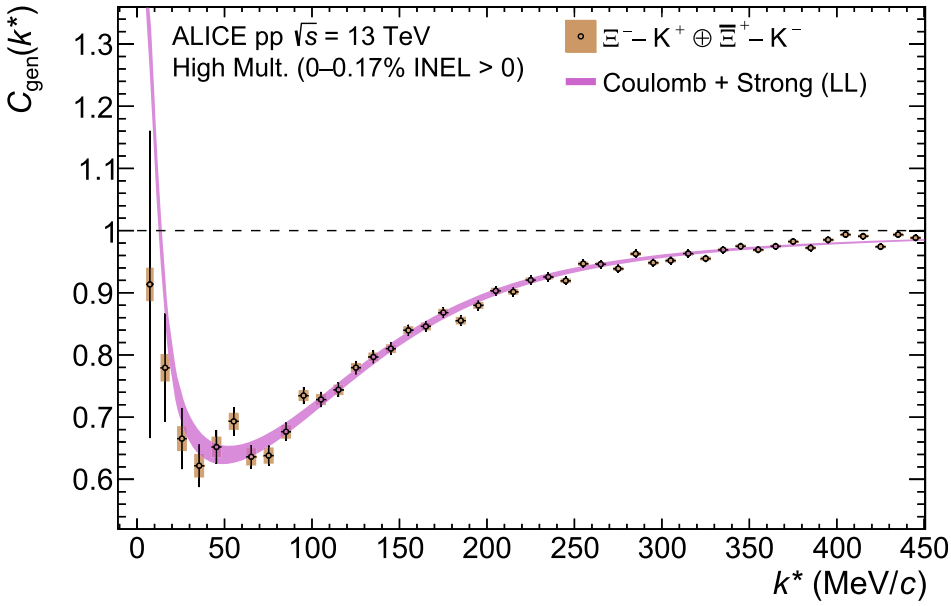

Fig. 2. Extracted genuine Ξ-K correlation (data points) and genuine theoretical correlation function with the LL approach (pink line). Statistical (black vertical lines) and systematic (orange boxes) uncertainties of the data are shown separately. See text for details.

take into account both the data systematic uncertainties (see Section 2), and the systematic variations of the fit. The genuine correlation function is compared with the genuine interaction part from the fit with the LL model (pink band) after consideration of the finite momentum resolution effects.

While the experimentally obtained $C_{\rm gen}(k^*)$ can be compared to any model of the Ξ-K interaction, given the source size reported in this work, it is important to note that its determination, and consequently the determination of the interaction parameters, inherently depends on the modeling of the mini-jet background baseline. Since this baseline is determined simultaneously with the interaction parameters during the fit to the total correlation function, its characterization directly influences the extracted strong interaction signal represented by $C_{\rm gen}(k^*)$.

5. Results on $\Xi - \pi$ correlations

The measured $\Xi - \pi$ correlation function is shown in Fig. 3. The pink and green bands depict the modeling of the total correlation function based on Eq. (2), incorporating genuine, residuals and background contributions. The influence of the $C_{\rm background}(k^*)$ contribution, highlighted in gray and multiplied by $N_{\rm D}$, is clearly visible in the deviation of data from unity, starting already at large k^* values. The width of the bands represents the total uncertainty of the fit, estimated analogously to the Ξ-K case, except for the exclusion of variations on the background shape. Uncertainties on the $\Xi - \pi$ background are included by a bootstrap sampling from the MC correlation template [93]. The fit range considered in the $\Xi - \pi$ case is $k^* \in [0, 1000]$ MeV/c. See full fit range figure in the Appendix A.

The $\Xi - \pi$ correlation function lies above unity in the low k^* region, indicating an overall attractive interaction between Ξ baryons and pions. A first scenario, shown by the green band, assumes a pure attraction coming from the Coulomb interaction and it clearly underestimates the data in the k^* region below the Ξ(1530) peak. With the inclusion of the strong potential, via the Lednický–Lyuboshits wavefunction approach discussed in Section 3, a better description of the data is achieved, particularly in this low k^* region. The extracted value of $\Re f_0 = 0.070 \pm 0.004(\text{stat.}) \pm 0.011(\text{syst.})$ fm confirms the need for an additional shallow strong attraction to describe the data. The $\Im f_0 = 0.002 \pm 0.003(\text{stat.}) \pm 0.010(\text{syst.})$ is compatible with zero. Such a result is expected since the $\Xi - \pi$ is the lowest energy channel that opens in the meson-baryon S = −2 sector. The values of f_0 obtained in this work are overall compatible with results on the $\Xi - \pi$ scattering length evaluated within UChPT in a coupled-channel approach in Ref. [11]. The improvement in the fit with the inclusion of a strong $\Xi - \pi$ interaction is estimated in terms of number of standard deviations $n\sigma$ between the data and the assumed model calculated over the full fit range. With the introduction of an additional strong attraction, the $n\sigma$ decreases to 15 from a value of 25 for the Coulomb-only scenario. A deviation between the assumed modeling and the data can be seen in the region below $k^* \approx 50$ MeV/c, with a clear overestimation of the measured correlation. Such a discrepancy might be caused by the need to include in the model higher-partial waves which could play a role in the $\Xi - \pi$ interacting potential already at low momenta, due to the appearance of the Ξ(1530) state. Indeed, a deviation above the 5σ level is also observed within the few data points around the k^* region of the Ξ(1530) peak, pointing as well to the need of an improved modeling of this state. More refined theoretical calculations, able to go beyond the s-wave assumption done in this work, could be useful in reducing the current disagreement.

As already discussed in Section 3, two additional neutral states are visible in the measured $\Xi - \pi$ correlation, just above the Ξ(1530) signal: the Ξ(1620) at $k^* \approx 240$ MeV/c and the Ξ(1690) at $k^* \approx 300$ MeV/c. Both these states are shown in detail in the inset of Fig. 3. The properties of these two excited Ξ* have been determined from the fit that yields: $M_{\Xi(1620)} = 1608.16 \pm 1.56(\text{stat.} + \text{syst.})$ MeV/c^2, $\Gamma_{\Xi(1620)} = 47.12 \pm 5.63(\text{stat.} + \text{syst.})$ MeV, $M_{\Xi(1690)} = 1680.72 \pm 3.27(\text{stat.} + \text{syst.})$ MeV/c^2, $\Gamma_{\Xi(1690)} = 26.41 \pm 13.86(\text{stat.} + \text{syst.})$ MeV. The mass and width obtained for the neutral Ξ(1690) state are in agreement with the reported PDG values [65] and with measurements by LHCb [15] and Belle [12] collaborations. For the much less known Ξ(1620) state, a lower mass value for the neutral state is extracted in comparison to the results obtained for the charged partner observed in the Λ–K⁻ correlation [23]. Such a trend is expected, and widely observed, in isospin doublets based on the slight breaking of isospin symmetry [65]. Compared with the Belle measurement in the same $\Xi - \pi$ channel, the mass value obtained from the $\Xi - \pi$ correlation is in agreement, while a narrower width is obtained, consistent with the results reported from Λ–K⁻ correlations [23].

Finally, it is worth mentioning a third structure present in the measured $\Xi - \pi$ correlation which appears at very large momenta. In the region of $850 < k^* < 950$ MeV/c, the peak of the produced Ξ_c^0 decaying into $\Xi - \pi$ (BR= $1.43 \pm 0.27\%$) is visible (see Fig. A.3 in Appendix A). In the

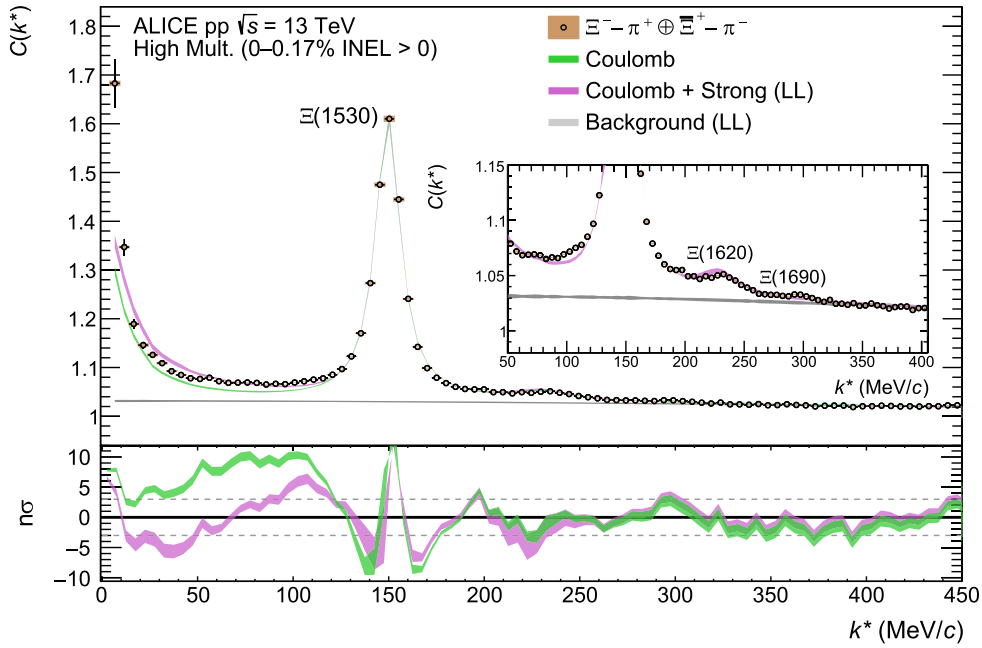

Fig. 3. Measured correlation function of $\Xi - \pi$ pairs. Statistical (bars) and systematic (boxes) uncertainties are shown separately. The pink band represents the fit with both Coulomb and strong interactions via the LL approach, while the green band indicates the Coulomb-only results. The $C_{\text{background}}(k^*)$ within the Coulomb + strong fit is reported in gray. The inset shows a zoomed-in view of the y-axis, highlighting the k^* region of the $\Xi(1620)$ and $\Xi(1690)$ states in greater detail. The lower panel presents the difference between the data and the modeled correlation functions using Coulomb and strong interactions (pink) and Coulomb only (green) expressed as the number of standard deviations, $n\sigma$.

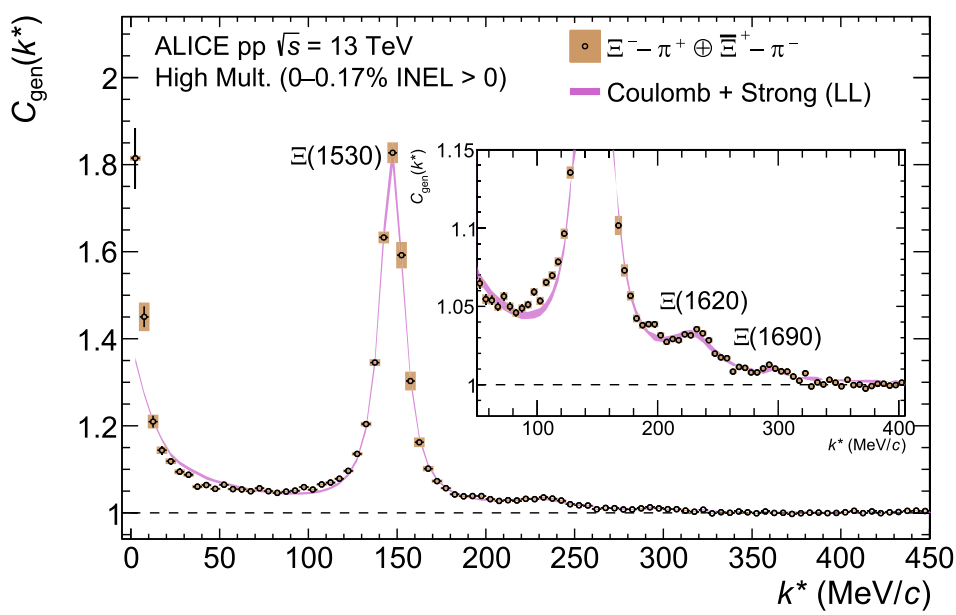

Fig. 4. Genuine $\Xi - \pi$ correlation function. Statistical (bars) and systematic (boxes) uncertainties are shown separately. The pink band represents the genuine theoretical correlation function obtained with both Coulomb and strong interactions. The inset shows a zoomed-in view of the y-axis, highlighting the k^* region of the $\Xi(1620)$ and $\Xi(1690)$ states in greater detail.

same k^* region, the PDG reports another heavy excited Ξ^* state, namely the $\Xi(2500)$. Currently this state is very poorly known, with no precise information reported on mass, width and quantum numbers. A test of the feasibility of delivering quantitative constraints on the $\Xi(2500)$ has been performed; however, the current femtoscopy data can be described solely by the presence of the signal from the Ξ_c^0 decay. Additional details on this test are reported in the Appendix A.

Fig. 4 showcases the extracted genuine $\Xi - \pi$ correlation, obtained in an analogous way to the Ξ-K pairs. The genuine $\Xi - \pi$ correlation is above unity, confirming the attractive nature of the $\Xi - \pi$ interaction, and it reaches unity just above the $\Xi(1690)$ state, indicating the robust treatment of the non-femtoscopic background thanks to the constrained MC template described in Section 3. The reported pink band represents the genuine theoretical correlation, corrected for momentum resolution effects, obtained assuming the above-mentioned $\Xi - \pi$ scattering length. In the inset, the $\Xi(1620)$ and $\Xi(1690)$ states are also shown and well reproduced by the considered model. The extraction of the genuine $\Xi - \pi$ correlation is free from the indetermination in the background descrip-

tion found in the case of Ξ-K, hence a model-independent set of high-precision data is delivered, covering a wide range of momenta, from the threshold up to 1 GeV/c.

6. Conclusions

In this work, high-precision data on oppositely charged Ξ-K and $\Xi-\pi$ interactions are presented via measurements of their correlation functions in HM ppcollisions at $\sqrt{s}$ = 13 TeV. Scattering parameters for both systems are extracted using the Lednický–Lyuboshits approximation for the wavefunction, indicating a repulsive strong interaction for Ξ-K and a shallow attraction for $\Xi-\pi$. The data presented in this work constitute a fundamental input in understanding the underlying strong interaction between multi-strange and light hadrons.

The Ξ-K correlation function provides new data in an energy region where direct scattering measurements are scarce. These results therefore impose an important constraint for theoretical models aiming to describe the meson-baryon interaction in the S = −1 sector. So far, the observed level of repulsion in the Ξ-K system is not fully captured by the current theoretical approaches, highlighting the necessity of further refinement in the theoretical understanding of these interactions. It is important to highlight that the coupling to the $\Lambda\pi$ channel is predicted to have a substantial influence on the final Ξ-K correlation function [52]. For this reason, it would be desirable to perform in the future a full coupled-channel analysis of the femtoscopy data in the S = −1 sector, aiming to simultaneously describe the high-precision ALICE data for K^-p correlations together with the Ξ-K data here presented, and forthcoming Λ–π correlations.

The properties of Ξ(1620) and Ξ(1690) states, visible in the measured $\Xi-\pi$ correlation function, are extracted and found to be overall compatible with previous measurements. Future measurements within the current LHC Run 3 and Run 4, aimed at a better understanding of the underlying coupled-channel dynamics in the S = −2 sector, should involve the challenging measurements of correlations involving $\Sigma\overline{K}$ pairs. Insights into these high energy channels could provide access to many heavy Ξ^* states, still poorly known.

Data availability

This manuscript has associated data in a HEPData repository at: https://www.hepdata.net/record/ins2974295.

Declaration of competing interest

The authors declare that they have no known competing financial interests or personal relationships that could have appeared to influence the work reported in this paper.

Acknowledgement

The ALICE Collaboration is grateful to Dr. A. Feijoo and P. Encarnación for the fruitful discussions and valuable guidance on the theoretical description.

The ALICE Collaboration would like to thank all its engineers and technicians for their invaluable contributions to the construction of the experiment and the CERN accelerator teams for the outstanding performance of the LHC complex. The ALICE Collaboration gratefully acknowledges the resources and support provided by all Grid centres and the Worldwide LHC Computing Grid (WLCG) collaboration. The ALICE Collaboration acknowledges the following funding agencies for their support in building and running the ALICE detector: A. I. Alikhanyan National Science Laboratory (Yerevan Physics Institute) Foundation (ANSL), State Committee of Science and World Federation of Scientists (WFS), Armenia; Austrian Academy of Sciences, Austrian Science Fund (FWF): [M 2467-N36] and Nationalstiftung für Forschung, Technologie und Entwicklung, Austria; Ministry of Communications and High Technologies, National Nuclear Research Center, Azerbaijan; Rede Nacional de Física de Altas Energias (Renafae), Financiadora de Estudos e Projetos (Finep), Fundação de Amparo à Pesquisa do Estado de São Paulo (FAPESP) and The Sao Paulo Research Foundation (FAPESP), Brazil; Bulgarian Ministry of Education and Science, within the National Roadmap for Research Infrastructures 2020–2027 (object CERN), Bulgaria; Ministry of Education of China (MOEC) , Ministry of Science & Technology of China (MSTC) and National Natural Science Foundation of China (NSFC), China; Ministry of Science and Education and Croatian Science Foundation, Croatia; Centro de Aplicaciones Tecnológicas y Desarrollo Nuclear (CEADEN), Cubaenergía, Cuba; Ministry of Education, Youth and Sports of the Czech Republic, Czech Republic; The Danish Council for Independent Research | Natural Sciences, the VILLUM FONDEN and Danish National Research Foundation (DNRF), Denmark; Helsinki Institute of Physics (HIP), Finland; Commissariat à l'Energie Atomique (CEA) and Institut National de Physique Nucléaire et de Physique des Particules (IN2P3) and Centre National de la Recherche Scientifique (CNRS), France; Bundesministerium für Forschung, Technologie und Raumfahrt (BMFTR) and GSI Helmholtzzentrum für Schwerionenforschung GmbH, Germany; General Secretariat for Research and Technology, Ministry of Education, Research and Religions, Greece; National Research, Development and Innovation Office, Hungary; Department of Atomic Energy Government of India (DAE), Department of Science and Technology, Government of India (DST), University Grants Commission, Government of India (UGC) and Council of Scientific and Industrial Research (CSIR), India; National Research and Innovation Agency - BRIN, Indonesia; Istituto Nazionale di Fisica Nucleare (INFN), Italy; Japanese Ministry of Education, Culture, Sports, Science and Technology (MEXT) and Japan Society for the Promotion of Science (JSPS) KAKENHI, Japan; Consejo Nacional de Ciencia (CONACYT) y Tecnología, through Fondo de Cooperación Internacional en Ciencia y Tecnología (FONCICYT) and Dirección General de Asuntos del Personal Academico (DGAPA), Mexico; Nederlandse Organisatie voor Wetenschappelijk Onderzoek (NWO), Netherlands; The Research Council of Norway, Norway; Pontificia Universidad Católica del Perú, Peru; Ministry of Science and Higher Education, National Science Centre and WUT ID-UB, Poland; Korea Institute of Science and Technology Information and National Research Foundation of Korea (NRF), Republic of Korea; Ministry of Education and Scientific Research, Institute of Atomic Physics, Ministry of Research and Innovation and Institute of Atomic Physics and Universitatea Nationala de Stiinta si Tehnologie Politehnica Bucuresti, Romania; Ministerstvo skolstva, vyskumu, vyvoja a mladeze SR, Slovakia; National Research Foundation of South Africa, South Africa; Swedish Research Council (VR) and Knut & Alice Wallenberg Foundation (KAW), Sweden; European Organization for Nuclear Research, Switzerland; Suranaree University of Technology (SUT), National Science and Technology Development Agency (NSTDA) and National Science, Research and Innovation Fund (NSRF via PMU-B B05F650021), Thailand; Turkish Energy, Nuclear and Mineral Research Agency (TENMAK), Turkey; National Academy of Sciences of Ukraine, Ukraine; Science and Technology Facilities Council (STFC), United Kingdom; National Science Foundation of the United States of America (NSF) and United States Department of Energy, Office of Nuclear Physics (DOE NP), United States of America. In addition, individual groups or members have received support from: Czech Science Foundation (grant no. 23-07499S), Czech Republic; FORTE project, reg. no. CZ.02.01.01/00/22_008/0004632, Czech Republic, co-funded by the European Union, Czech Republic; European Research Council (grant no. 950692), European Union; Deutsche Forschungs Gemeinschaft (DFG, German Research Foundation) "Neutrinos and Dark Matter in Astro- and Particle Physics" (grant no. SFB 1258), Germany; FAIR - Future Artificial Intelligence Research, funded by the NextGenerationEU program (Italy).

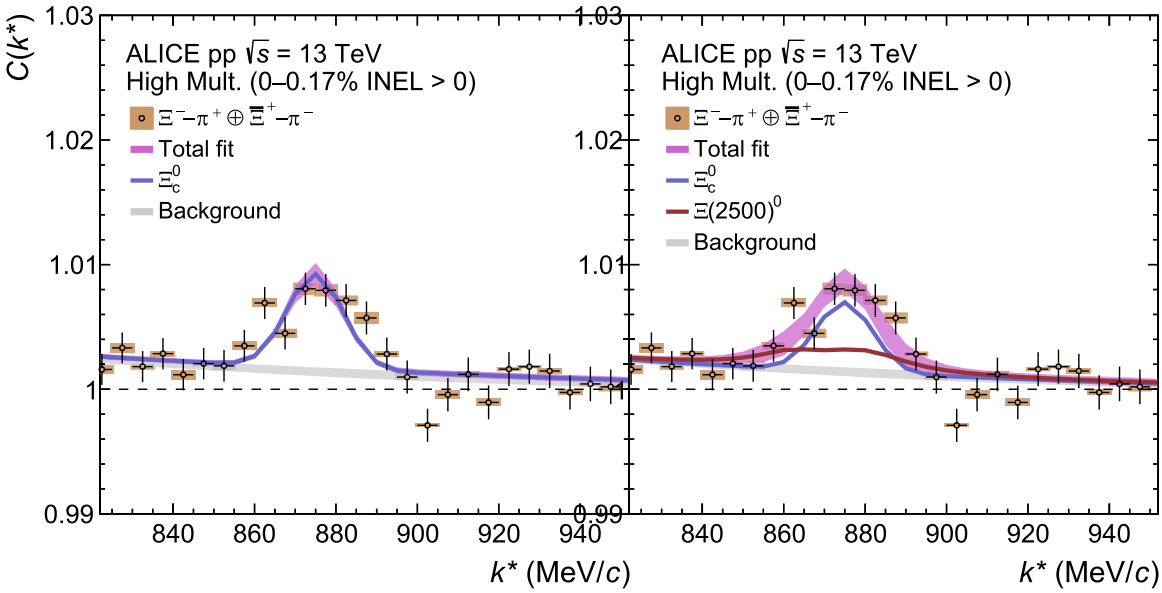

Fig. A.1. Region of the measured $\Xi - \pi$ correlation corresponding to the production of Ξ_c^0 decaying into $\Xi - \pi$ pairs. Left: results assuming only the presence of the Ξ_c state. Right: results assuming also the presence of the $\Xi(2500)$ state. The pink band represents the fit with Eq. (A.1), the polynomial background is given by the grey band. In blue and red, the center values of the profile shape of the $\Xi(2500)$ and Ξ_c^0 are shown, respectively.

Appendix A. Additional material

A.1. Results on Ξ(2500) state

In this section, more details on the study performed on $\Xi - \pi$ pairs in the region of k^* between 830 and 920 MeV/c are provided, where a structure corresponding to the produced $\Xi_c \to \Xi\pi$ resonance is visible. In the same region, an excited cascade, the $\Xi(2500)$, is expected to be present. This state is currently poorly known, with one-star PDG rating [65]. The PDG is reporting only an approximate value of the mass ($\approx 2500\,\mathrm{MeV}/c^2$) and the related references are mainly experimental searches using kaon beams conducted in the early seventies and eighties [94–96].

A chi-squared based likelihood test is conducted in the region $k^* \in [750 - 950]\mathrm{MeV}/c$ by fitting the structure visible in Fig. A.1 assuming either the only presence of the Ξ_c or adding as well the $\Xi(2500)$ state. In an attempt to extract properties of the $\Xi(2500)$ state, the known Ξ_c state is used as a constraint, i.e. it is included in the fit with fixed mass and width to its PDG nominal values [65]. Since the Ξ_c state is extremely narrow ($\Gamma \approx 10^{-6}$ MeV), a Monte Carlo simulation was performed in order to evaluate the effect of the k^* momentum resolution on the original distribution. The momentum smearing matrix, relating the original "true" k^*_{true} to the reconstructed k^*_{reco} one, is taken as initial input, limited to the region of interest in k^*. From the latter, at each value of k^*_{true}, a corresponding Gaussian distribution in k^*_{reco} provides the mean $\langle k^*_{\mathrm{reco}} \rangle$ value and $\sigma_{k^*_{\mathrm{reco}}}$ dispersion. As expected, the width of the Ξ_c^0 is fully dominated by the resolution in k^*, found to be equal to $\Gamma_{\Xi_c} = \sigma_{\mathrm{res.}} = 6.9$ MeV/c.

The function used to perform the fit reads

$$f_{\mathrm{fit}}(k^*) = B_{\mathrm{pol2}}(k^*) + A \cdot \left[w_{\Xi_c} f^G_{\Xi_c}(M_{\Xi_c}, \Gamma_{\Xi_c}) + w_{\Xi(2500)} f^{BW}_{\Xi(2500)}(M_{\Xi(2500)}, \Gamma_{\Xi(2500)}) \right], \quad \text{(A.1)}$$

in which the free parameters to be determined in the fit are the ones related to the polynomial background $B_{\mathrm{pol2}}(k^*) = a_0(1 + a_1 k^* + a_2 (k^*)^2)$, A, w_{Ξ_c}, $w_{\Xi(2500)}$, $M_{\Xi(2500)}$ and $\Gamma_{\Xi(2500)}$. The Ξ_c is modeled via a Gaussian distribution with fixed width $\Gamma_{\Xi_c} = \sigma_{\mathrm{res.}}$ and fixed mass to the PDG value, $M_{\Xi_c} = 2470.4$ MeV (corresponding to $k^* = 874.7$ MeV/c) [65]. The corresponding distribution is shown in blue in both panels of Fig. A.1. A Breit-Wigner distribution is employed for the $\Xi(2500)$, with mass $M_{\Xi(2500)}$ and width $\Gamma_{\Xi(2500)}$ to be extracted from the comparison to data.

Two scenarios have been tested in order to probe the sensitivity to the presence of the $\Xi(2500)$ state. In the left panel of Fig. A.1, the fit assuming only the Ξ_c state is shown, using Eq. (A.1) with $w_{\Xi(2500)} = 0$, and a reduced chi-square of 1.99 is obtained. On the right panel of Fig. A.1, the results with the additional inclusion of the $\Xi(2500)$ state are presented for completeness. The limits of variation for the mass and width of the $\Xi(2500)$ are taken from the lower and upper limits provided by the previous measurements as listed by the PDG (see Refs. [94–96]). In red, the obtained shape of the $\Xi(2500)$ state, scaled by its weight $w_{\Xi(2500)}$, is also reported. The extracted values of mass and width are $M_{\Xi(2500)} = 2469.0 \pm 14.3$ (stat. + syst.) MeV/c^2 and $\Gamma_{\Xi(2500)} = 32.0 \pm 22.2$ (stat. + syst.) MeV. In this case, a reduced chi-square of 2.07 is achieved, therefore indicating that within the current experimental precision, the presence of the $\Xi(2500)$ state is not necessary to describe the data.

A.2. Full fit range correlation functions for Ξ-K and Ξ − π pairs

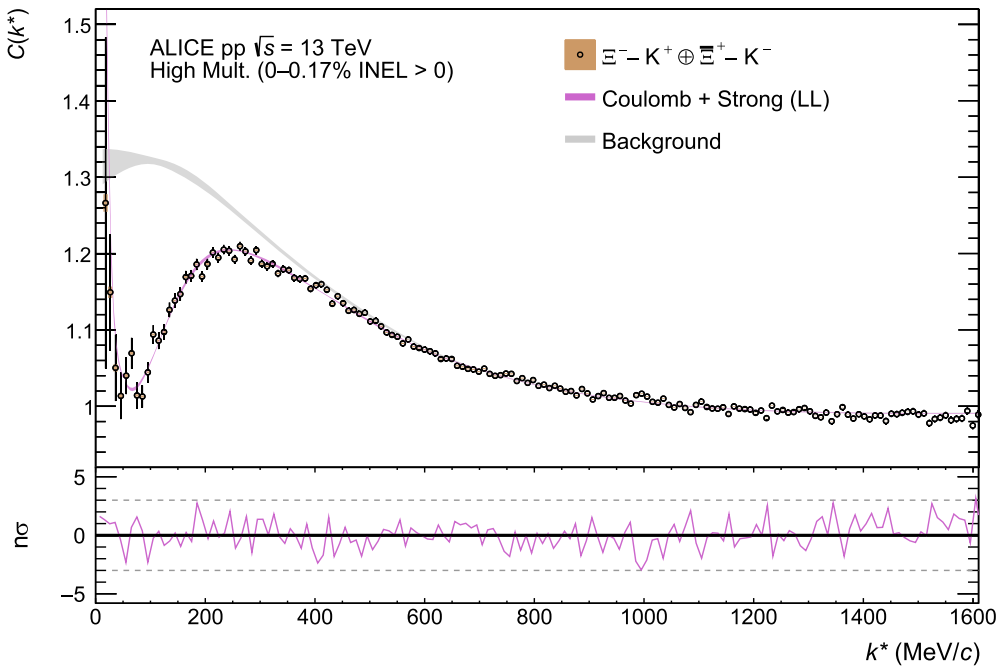

Fig. A.2. Measured correlation function of Ξ-K pairs in the whole fit range. Statistical (bars) and systematic (boxes) uncertainties are shown separately. The pink band represents the fit with both Coulomb and strong interaction using the LL method. The $C_{\text{background}}(k^*)$ multiplied by the normalization constant N_D obtained within the Coulomb + strong fit is reported in gray.

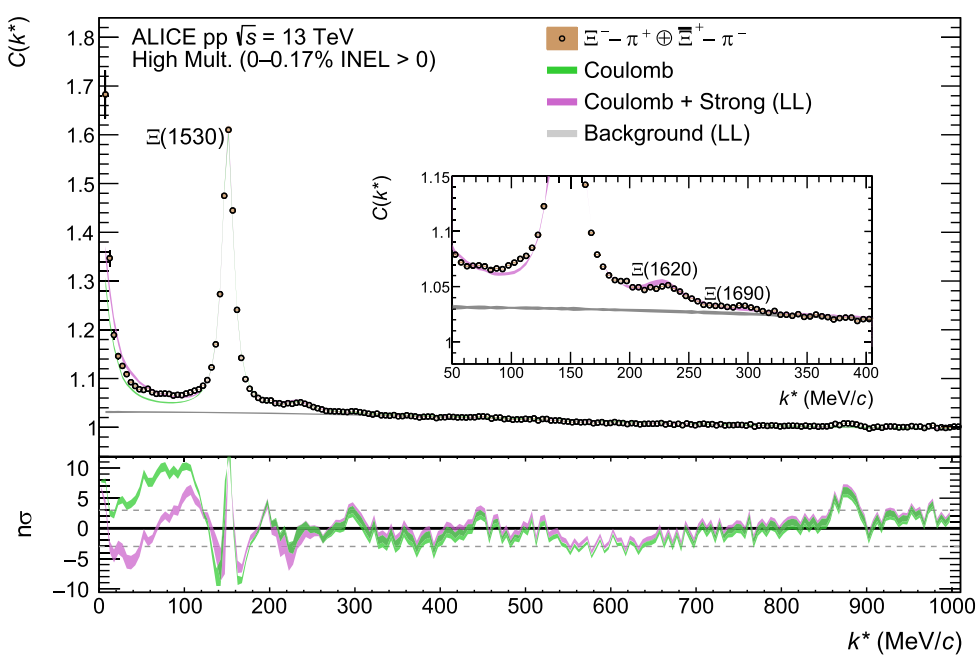

Fig. A.3. Measured correlation function of Ξ − π pairs in the whole fit range. Statistical (bars) and systematic (boxes) uncertainties are shown separately. The pink band represents the fit with both Coulomb and strong interaction using the LL method,. The $C_{\text{background}}(k^*)$ multiplied by the normalization constant N_D obtained within the Coulomb + strong fit is reported in gray. The inset shows a zoomed-in view of the y-axis, highlighting the k^* region of the Ξ(1620) and Ξ(1690) states in greater detail.

Appendix B. The ALICE Collaboration

ALICE Collaboration

I.J. Abualrob[114], S. Acharya[50], G. Aglieri Rinella[32], L. Aglietta[24], N. Agrawal[25], Z. Ahammed[134], S. Ahmad[15], I. Ahuja[36], Z.U.L. Akbar[81], A. Akindinov[140], V. Akishina[38], M. Al-Turany[96], D. Aleksandrov[140], B. Alessandro[56], R. Alfaro Molina[67], B. Ali[15], A. Alici[25], A. Alkin[102], J. Alme[20], G. Alocco[24], T. Alt[64], I. Altsybeev[94], C. Andrei[45], N. Andreou[113], A. Andronic[125], E. Andronov[140], M. Angeletti[32], V. Anguelov[93], F. Antinori[54], P. Antonioli[51], N. Apadula[72], H. Appelshäuser[64], S. Arcelli[25], R. Arnaldi[56], J.G.M.C.A. Arneiro[108], I.C. Arsene[19], M. Arslandok[137], A. Augustinus[32], R. Averbeck[96], M.D. Azmi[15], H. Baba[123], A.R.J. Babu[136], A. Badalà[53], J. Bae[102], Y. Bae[102], Y.W. Baek[40], X. Bai[118], R. Bailhache[64], Y. Bailung[48], R. Bala[90], A. Baldisseri[129], B. Balis[2], S. Bangalia[116], Z. Banoo[90], V. Barbasova[36], F. Barile[31], L. Barioglio[56], M. Barlou[24,77], B. Barman[41], G.G. Barnaföldi[46], L.S. Barnby[113], E. Barreau[101], V. Barret[126], L. Barreto[108], K. Barth[32], E. Bartsch[64], N. Bastid[126], G. Batigne[101], D. Battistini[94], B. Batyunya[141], D. Bauri[47], J.L. Bazo Alba[100], I.G. Bearden[82], P. Becht[96], D. Behera[48], S. Behera[47], I. Belikov[128], V.D. Bella[128], F. Bellini[25], R. Bellwied[114], L.G.E. Beltran[107], Y.A.V. Beltran[44], G. Bencedi[46], A. Bensaoula[114], S. Beole[24], Y. Berdnikov[140], A. Berdnikova[93], L. Bergmann[72,93], L. Bernardinis[23], L. Betev[32], P.P. Bhaduri[134], T. Bhalla[89], A. Bhasin[90], B. Bhattacharjee[41], S. Bhattarai[116], L. Bianchi[24], J. Bielčík[34], J. Bielčíková[85], A. Bilandzic[94], A. Binoy[116], G. Biro[46], S. Biswas[4], D. Blau[140], M.B. Blidaru[96], N. Bluhme[38], C. Blume[64], F. Bock[86], T. Bodova[20], L. Boldizsár[46], M. Bombara[36], P.M. Bond[32], G. Bonomi[133,55], H. Borel[129], A. Borissov[140], A.G. Borquez Carcamo[93], E. Botta[24], Y.E.M. Bouziani[64], D.C. Brandibur[63], L. Bratrud[64], P. Braun-Munzinger[96], M. Bregant[108], M. Broz[34], G.E. Bruno[95,31], V.D. Buchakchiev[35], M.D. Buckland[84], H. Buesching[64], S. Bufalino[29], P. Buhler[74], N. Burmasov[141], Z. Buthelezi[68,122], A. Bylinkin[20], C. Carr[99], J.C. Cabanillas Noris[107], M.F.T. Cabrera[114], H. Caines[137], A. Caliva[28], E. Calvo Villar[100], J.M.M. Camacho[107], P. Camerini[23], M.T. Camerlingo[50], F.D.M. Canedo[108], S. Cannito[23], S.L. Cantway[137], M. Carabas[111], F. Carnesecchi[32], L.A.D. Carvalho[108], J. Castillo Castellanos[129], M. Castoldi[32], F. Catalano[32], S. Cattaruzzi[23], R. Cerri[24], I. Chakaberia[72], P. Chakraborty[135], J.W.O. Chan[114], S. Chandra[134], S. Chapeland[32], M. Chartier[117], S. Chattopadhay[134], M. Chen[39], T. Cheng[6], C. Cheshkov[127], D. Chiappara[27], V. Chibante Barroso[32], D.D. Chinellato[74], F. Chinu[24], E.S. Chizzali[I,94], J. Cho[58], S. Cho[58], P. Chochula[32], Z.A. Chochulska[II,135], P. Christakoglou[83], C.H. Christensen[82], P. Christiansen[73], T. Chujo[124], M. Ciacco[24], C. Cicalo[52], G. Cimador[24], F. Cindolo[51], F. Colamaria[50], D. Colella[31], A. Colelli[31], M. Colocci[25], M. Concas[32], G. Conesa Balbastre[71], Z. Conesa del Valle[130], G. Contin[23], J.G. Contreras[34], M.L. Coquet[101], P. Cortese[132,56], M.R. Cosentino[110], F. Costa[32], S. Costanza[21], P. Crochet[126], M.M. Czarnynoga[135], A. Dainese[54], G. Dange[38], M.C. Danisch[16], A. Danu[63], A. Daribayeva[38], P. Das[32], S. Das[4], A.R. Dash[125], S. Dash[47], A. De Caro[28], G. de Cataldo[50], J. de Cuveland[38], A. De Falco[22], D. De Gruttola[28], N. De Marco[56], C. De Martin[23], S. De Pasquale[28], R. Deb[133], R. Del Grande[94], L. Dello Stritto[32], G.G.A. de Souza[III,108], P. Dhankher[18], D. Di Bari[31], M. Di Costanzo[29], A. Di Mauro[32], B. Di Ruzza[131,50], B. Diab[32], Y. Ding[6], J. Ditzel[64], R. Divià[32], U. Dmitrieva[56], A. Dobrin[63], B. Dönigus[64], L. Döpper[42], J.M. Dubinski[135], A. Dubla[96], P. Dupieux[126], N. Dzalaiova[13], T.M. Eder[125], R.J. Ehlers[72], F. Eisenhut[64], R. Ejima[91], D. Elia[50], B. Erazmus[101], F. Ercolessi[25], B. Espagnon[130], G. Eulisse[32], D. Evans[99], L. Fabbietti[94], M. Faggin[32], J. Faivre[71], F. Fan[6], W. Fan[114], T. Fang[6], A. Fantoni[49], M. Fasel[86], A. Feliciello[56], G. Feofilov[140], A. Fernández Téllez[44], L. Ferrandi[108], A. Ferrero[129], C. Ferrero[IV,56], A. Ferretti[24], V.J.G. Feuillard[93], D. Finogeev[141], F.M. Fionda[52], A.N. Flores[106], S. Foertsch[68], I. Fokin[93], S. Fokin[140], U. Follo[IV,56], R. Forynski[113], E. Fragiacomo[57], H. Fribert[94], U. Fuchs[32], N. Funicello[28], C. Furget[71], A. Furs[141], T. Fusayasu[97], J.J. Gaardhøje[82], M. Gagliardi[24], A.M. Gago[100], T. Gahlaut[47], C.D. Galvan[107], S. Gami[79], P. Ganoti[77], C. Garabatos[96], J.M. Garcia[44], T. García Chávez[44], E. Garcia-Solis[9], S. Garetti[130], C. Gargiulo[32], P. Gasik[96], H.M. Gaur[38], A. Gautam[116], M.B. Gay Ducati[66], M. Germain[101], R.A. Gernhaeuser[94], C. Ghosh[134], M. Giacalone[32], G. Gioachin[29], S.K. Giri[134], P. Giubellino[56], P. Giubilato[27], P. Glässel[93], E. Glimos[121], L. Gonella[23], V. Gonzalez[136], M. Gorgon[2], K. Goswami[48], S. Gotovac[33], V. Grabski[67], L.K. Graczykowski[135], E. Grecka[85], A. Grelli[59], C. Grigoras[32], V. Grigoriev[140], S. Grigoryan[141,1], O.S. Groettvik[32], F. Grosa[32], S. Gross-Bölting[96], J.F. Grosse-Oetringhaus[32], R. Grosso[96], D. Grund[34], N.A. Grunwald[93], R. Guernane[71], M. Guilbaud[101], K. Gulbrandsen[82], J.K. Gumprecht[74], T. Gündem[64], T. Gunji[123], J. Guo[10], W. Guo[6], A. Gupta[90], R. Gupta[90], R. Gupta[48], K. Gwizdziel[135], L. Gyulai[46], C. Hadjidakis[130], F.U. Haider[90], S. Haidlova[34], M. Haldar[4], H. Hamagaki[75], Y. Han[139], B.G. Hanley[136], R. Hannigan[106], J. Hansen[73], J.W. Harris[137], A. Harton[9], M.V. Hartung[64], A. Hasan[120], H. Hassan[115], D. Hatzifotiadou[51], P. Hauer[42], L.B. Havener[137], E. Hellbär[32], H. Helstrup[37], M. Hemmer[64], T. Herman[34], S.G. Hernandez[114], G. Herrera Corral[8], K.F. Hetland[37], B. Heybeck[64], H. Hillemanns[32], B. Hippolyte[128], I.P.M. Hobus[83], F.W. Hoffmann[38], B. Hofman[59], M. Horst[94], A. Horzyk[2], Y. Hou[96,11,6], P. Hristov[32], P. Huhn[64], L.M. Huhta[115], T.J. Humanic[87], V. Humlova[34], A. Hutson[114], D. Hutter[38], M.C. Hwang[18], R. Ilkaev[140], M. Inaba[124], M. Ippolitov[140], A. Isakov[83], T. Isidori[116], M.S. Islam[47], M. Ivanov[13], M. Ivanov[96], K.E. Iversen[73], J.G. Kim[139], M. Jablonski[2], B. Jacak[18,72], N. Jacazio[25], P.M. Jacobs[72], A. Jadlovska[104], S. Jadlovska[104], S. Jaelani[81], C. Jahnke[109], M.J. Jakubowska[135], E.P. Jamro[2], D.M. Janik[34], M.A. Janik[135], S. Ji[16], Y. Ji[96], S. Jia[82], T. Jiang[10], A.A.P. Jimenez[65], S. Jin[10], F. Jonas[72], D.M. Jones[117], J.M. Jowett [32,96], J. Jung[64], M. Jung[64], A. Junique[32], A. Jusko[99], J. Kaewjai[103], P. Kalinak[60], A. Kalweit[32], A. Karasu Uysal[138], N. Karatzenis[99], O. Karavichev[140], T. Karavicheva[140], M.J. Karwowska[135], V. Kashyap[79], M. Keil[32], B. Ketzer[42], J. Keul[64], S.S. Khade[48], A.M. Khan[118], A. Khanzadeev[140], Y. Kharlov[140], A. Khatun[116], A. Khuntia[51], Z. Khuranova[64], B. Kileng[37], B. Kim[102], D.J. Kim[115], D. Kim[102], E.J. Kim[69], G. Kim[58], H. Kim[58], J. Kim[139], J. Kim[58], J. Kim[32], M. Kim[18], S. Kim[17], T. Kim[139], K. Kimura[91], J.T. Kinner[125], S. Kirsch[64], I. Kisel[38], S. Kiselev[140], A. Kisiel[135], J.L. Klay[5], J. Klein[32], S. Klein[72], C. Klein-Bösing[125], M. Kleiner[64], A. Kluge[32], M.B. Knuesel[137], C. Kobdaj[103], R. Kohara[123], A. Kondratyev[141], N. Kondratyeva[140], J. Konig[64], P.J. Konopka[32], G. Kornakov[135], M. Korwieser[94], S.D. Koryciak[2], C. Koster[83], A. Kotliarov[85], N. Kovacic[88], V. Kovalenko[140], M. Kowalski[105], V. Kozhuharov[35], G. Kozlov[38], I. Králik[60], A. Kravčáková[36], L. Krcal[32], M. Krivda[99,60], F. Krizek[85], K. Krizkova Gajdosova[34], C. Krug[66], M. Krüger[64], E. Kryshen[140], V. Kučera[58], C. Kuhn[128], T. Kumaoka[124], D. Kumar[134], L. Kumar[89], N. Kumar[89], S. Kumar[50], S. Kundu[32], M. Kuo[124], P. Kurashvili[78], A.B. Kurepin[140], S. Kurita[91], A. Kuryakin[140], S. Kushpil[85], A. Kuznetsov[141], M.J. Kweon[58], Y. Kwon[139], S.L. La Pointe[38], P. La Rocca[26], A. Lakrathok[103], S. Lambert[101], A.R. Landou[71], R. Langoy[120], E. Laudi[32], L. Lautner[94], R.A.N. Laveaga[107], R. Lavicka[74], R. Lea[133,55], J.B. Lebert[38], H. Lee[102], I. Legrand[45], G. Legras[125], A.M. Lejeune[34], T.M. Lelek[2], I. León Monzón[107], M.M. Lesch[94], P. Lévai[46], M. Li[6], P. Li[10], X. Li[10], B.E. Liang-Gilman[18], J. Lien[120], R. Lietava[99], I. Likmeta[114], B. Lim[56], H. Lim[16],

S.H. Lim[16], S. Lin[10], V. Lindenstruth[38], C. Lippmann[96], D. Liskova[104], D.H. Liu[6], J. Liu[117], G.S.S. Liveraro[109], I.M. Lofnes[20], C. Loizides[86], S. Lokos[105], J. Lömker[59], X. Lopez[126], E. López Torres[7], C. Lotteau[127], P. Lu[118], W. Lu[6], Z. Lu[10], O. Lubynets[96], F.V. Lugo[67], J. Luo[39], G. Luparello[57], M.A.T. Johnson[44], J. M. Friedrich[94], Y.G. Ma[39], M. Mager[32], A. Maire[128], E.M. Majerz[2], M.V. Makariev[35], G. Malfattore[51], N.M. Malik[90], N. Malik[15], S.K. Malik[90], D. Mallick[130], N. Mallick[115], G. Mandaglio[30,53], S.K. Mandal[78], A. Manea[63], R.S. Manhart[94], V. Manko[140], A.K. Manna[48], F. Manso[126], G. Mantzaridis[94], V. Manzari[50], Y. Mao[6], R.W. Marcjan[2], G.V. Margagliotti[23], A. Margotti[51], A. Marín[96], C. Markert[106], P. Martinengo[32], M.I. Martínez[44], M.P.P. Martins[32,108], S. Masciocchi[96], M. Masera[24], A. Masoni[52], L. Massacrier[130], O. Massen[59], A. Mastroserio[131,50], L. Mattei[24,126], S. Mattiazzo[27], A. Matyja[105], J.L. Mayo[106], F. Mazzaschi[32], M. Mazzilli[31,114], Y. Melikyan[43], M. Melo[108], A. Menchaca-Rocha[67], J.E.M. Mendez[65], E. Meninno[74], M.W. Menzel[32,93], M. Meres[13], L. Micheletti[56], D. Mihai[111], D.L. Mihaylov[94], A.U. Mikalsen[20], K. Mikhaylov[141,140], L. Millot[71], N. Minafra[116], D. Miśkowiec[96], A. Modak[57,133], B. Mohanty[79], M. Mohisin Khan[15,V], M.A. Molander[43], M.M. Mondal[79], S. Monira[135], D.A. Moreira De Godoy[125], A. Morsch[32], T. Mrnjavac[32], S. Mrozinski[64], V. Muccifora[49], S. Muhuri[134], A. Mulliri[22], M.G. Munhoz[108], R.H. Munzer[64], H. Murakami[123], L. Musa[32], J. Musinsky[60], J.W. Myrcha[135], B. Naik[122], A.I. Nambrath[18], B.K. Nandi[47], R. Nania[51], E. Nappi[50], A.F. Nassirpour[17], V. Nastase[111], A. Nath[93], N.F. Nathanson[82], K. Naumov[18], A. Neagu[19], L. Nellen[65], R. Nepeivoda[73], S. Nese[19], N. Nicassio[31], B.S. Nielsen[82], E.G. Nielsen[82], S. Nikolaev[140], V. Nikulin[140], F. Noferini[51], S. Noh[12], P. Nomokonov[141], J. Norman[117], N. Novitzky[86], A. Nyanin[140], J. Nystrand[20], M.R. Ockleton[117], M. Ogino[75], J. Oh[16], S. Oh[17], A. Ohlson[73], M. Oida[91], V.A. Okorokov[140], C. Oppedisano[56], A. Ortiz Velasquez[65], H. Osanai[75], J. Otwinowski[105], M. Oya[91], K. Oyama[75], S. Padhan[133,47], D. Pagano[133,55], G. Paić[65], S. Paisano-Guzmán[44], A. Palasciano[95,50], I. Panasenko[73], P. Panigrahi[47], C. Pantouvakis[27], H. Park[124], J. Park[124], S. Park[102], T.Y. Park[139], J.E. Parkkila[135], P.B. Pati[82], Y. Patley[47], R.N. Patra[50], P. Paudel[116], B. Paul[134], H. Pei[6], T. Peitzmann[59], X. Peng[54,11], M. Pennisi[24], S. Perciballi[24], D. Peresunko[140], G.M. Perez[7], Y. Pestov[140], M. Petrovici[45], S. Piano[57], M. Pikna[13], P. Pillot[101], O. Pinazza[51,32], C. Pinto[32], S. Pisano[49], M. Płoskoń[72], M. Planinic[88], D.K. Plociennik[2], M.G. Poghosyan[86], B. Polichtchouk[140], S. Politano[32], N. Poljak[88], A. Pop[45], S. Porteboeuf-Houssais[126], J.S. Potgieter[112], I.Y. Pozos[44], K.K. Pradhan[48], S.K. Prasad[4], S. Prasad[48], R. Preghenella[51], F. Prino[56], C.A. Pruneau[136], I. Pshenichnov[140], M. Puccio[32], S. Pucillo[28,24], S. Pulawski[119], L. Quaglia[24], A.M.K. Radhakrishnan[48], S. Ragoni[14], A. Rai[137], A. Rakotozafindrabe[129], N. Ramasubramanian[127], L. Ramello[132,56], C.O. Ramírez-Álvarez[44], M. Rasa[26], S.S. Räsänen[43], R. Rath[96], M.P. Rauch[20], I. Ravasenga[32], K.F. Read[86,121], C. Reckziegel[110], A.R. Redelbach[38], K. Redlich[VI,78], C.A. Reetz[96], H.D. Regules-Medel[44], A. Rehman[20], F. Reidt[32], H.A. Reme-Ness[37], K. Reygers[93], R. Ricci[28], M. Richter[20], A.A. Riedel[94], W. Riegler[32], A.G. Riffero[24], M. Rignanese[27], C. Ripoli[28], C. Ristea[63], M.V. Rodriguez[32], M. Rodríguez Cahuantzi[44], K. Røed[19], R. Rogalev[140], E. Rogochaya[141], D. Rohr[32], D. Röhrich[20], S. Rojas Torres[34], P.S. Rokita[135], G. Romanenko[25], F. Ronchetti[32], D. Rosales Herrera[44], E.D. Rosas[65], K. Roslon[135], A. Rossi[54], A. Roy[48], S. Roy[47], N. Rubini[51], J.A. Rudolph[83], D. Ruggiano[135], R. Rui[23], P.G. Russek[2], A. Rustamov[80], Y. Ryabov[140], A. Rybicki[105], L.C.V. Ryder[116], G. Ryu[70], J. Ryu[16], W. Rzesa[94,135], B. Sabiu[51], R. Sadek[72], S. Sadhu[42], S. Sadovsky[140], A. Saha[31], S. Saha[79], B. Sahoo[48], R. Sahoo[48], D. Sahu[65], P.K. Sahu[61], J. Saini[134], S. Sakai[124], S. Sambyal[90], D. Samitz[74], I. Sanna[32], T.B. Saramela[108], D. Sarkar[82], V. Sarritzu[22], V.M. Sarti[94], U. Savino[24], S. Sawan[79], E. Scapparone[51], J. Schambach[86], H.S. Scheid[32], C. Schiaua[45], R. Schicker[93], F. Schlepper[32,93], A. Schmah[96], C. Schmidt[96], M. Schmidt[92], N.V. Schmidt[86], J. Schoengarth[64], R. Schotter[74], A. Schröter[38], J. Schukraft[32], K. Schweda[96], G. Scioli[25], E. Scomparin[56], J.E. Seger[14], Y. Sekiguchi[123], D. Sekihata[123], M. Selina[83], I. Selyuzhenkov[96], S. Senyukov[128], J.J. Seo[93], D. Serebryakov[140], L. Serkin[VII,65], L. Šerkšnytė[94], A. Sevcenco[63], T.J. Shaba[68], A. Shabetai[101], R. Shahoyan[32], B. Sharma[90], D. Sharma[47], H. Sharma[54], M. Sharma[90], S. Sharma[90], T. Sharma[41], U. Sharma[90], O. Sheibani[136], K. Shigaki[91], M. Shimomura[76], S. Shirinkin[140], Q. Shou[39], Y. Sibiriak[140], S. Siddhanta[52], T. Siemiarczuk[78], T.F. Silva[108], W.D. Silva[108], D. Silvermyr[73], T. Simantathammakul[103], R. Simeonov[35], B. Singh[90], B. Singh[94], K. Singh[48], R. Singh[79], R. Singh[54,96], S. Singh[15], V.K. Singh[134], V. Singhal[134], T. Sinha[98], B. Sitar[13], M. Sitta[132,56], T.B. Skaali[19], G. Skorodumovs[93], N. Smirnov[137], K.L. Smith[16], R.J.M. Snellings[59], E.H. Solheim[19], C. Sonnabend[32,96], J.M. Sonneveld[83], F. Soramel[27], A.B. Soto-Hernandez[87], R. Spijkers[83], C. Sporleder[115], I. Sputowska[105], J. Staa[73], J. Stachel[93], I. Stan[63], T. Stellhorn[125], S.F. Stiefelmaier[93], D. Stocco[101], I. Storehaug[19], N.J. Strangmann[64], P. Stratmann[125], S. Strazzi[25], A. Sturniolo[30,53], A.A.P. Suaide[108], C. Suire[130], A. Suiu[111], M. Sukhanov[141], M. Suljic[32], R. Sultanov[140], V. Sumberia[90], S. Sumowidagdo[81], N.B. Sundstrom[59], L.H. Tabares[7], S.F. Taghavi[94], J. Takahashi[109], G.J. Tambave[79], Z. Tang[118], J. Tanwar[89], J.D. Tapia Takaki[116], N. Tapus[111], L.A. Tarasovicova[36], M.G. Tarzila[45], A. Tauro[32], A. Tavira García[130], G. Tejeda Muñoz[44], L. Terlizzi[24], C. Terrevoli[50], D. Thakur[24], S. Thakur[4], M. Thogersen[19], D. Thomas[106], N. Tiltmann[32,125], A.R. Timmins[114], A. Toia[64], R. Tokumoto[91], S. Tomassini[25], K. Tomohiro[91], N. Topilskaya[140], V.V. Torres[101], A. Trifiró[30,53], T. Triloki[95], A.S. Triolo[32,53], S. Tripathy[32], T. Tripathy[126], S. Trogolo[24], V. Trubnikov[3], W.H. Trzaska[115], T.P. Trzcinski[135], C. Tsolanta[19], R. Tu[39], A. Tumkin[140], R. Turrisi[54], T.S. Tveter[19], K. Ullaland[20], B. Ulukutlu[94], S. Upadhyaya[105], A. Uras[127], M. Urioni[23], G.L. Usai[22], M. Vaid[90], M. Vala[36], N. Valle[55], L.V.R. van Doremalen[59], M. van Leeuwen[83], C.A. van Veen[93], R.J.G. van Weelden[83], D. Varga[46], Z. Varga[137], P. Vargas Torres[65], M. Vasileiou[77], O. Vázquez Doce[49], O. Vazquez Rueda[114], V. Vechernin[140], P. Veen[129], E. Vercellin[24], R. Verma[47], R. Vértesi[46], M. Verweij[59], L. Vickovic[33], Z. Vilakazi[122], A. Villani[23], A. Vinogradov[140], T. Virgili[28], M.M.O. Virta[115], A. Vodopyanov[141], M.A. Völkl[99], S.A. Voloshin[136], G. Volpe[31], B. von Haller[32], I. Vorobyev[32], N. Vozniuk[141], J. Vrláková[36], J. Wan[39], C. Wang[39], D. Wang[39], Y. Wang[39], Y. Wang[6], Z. Wang[39], F. Weiglhofer[32,38], S.C. Wenzel[32], J.P. Wessels[125], P.K. Wiacek[2], J. Wiechula[64], J. Wikne[19], G. Wilk[78], J. Wilkinson[96], G.A. Willems[125], B. Windelband[93], J. Witte[93], M. Wojnar[2], J.R. Wright[106], C.-T. Wu[6,27], W. Wu[94,39], Y. Wu[118], K. Xiong[39], Z. Xiong[118], L. Xu[127,6], R. Xu[6], A. Yadav[42], A.K. Yadav[134], Y. Yamaguchi[91], S. Yang[58], S. Yang[20], S. Yano[91], Z. Ye[72], E.R. Yeats[18], J. Yi[6], R. Yin[39], Z. Yin[6], I.-K. Yoo[16], J.H. Yoon[58], H. Yu[12], S. Yuan[20], A. Yuncu[93], V. Zaccolo[23], C. Zampolli[32], F. Zanone[93], N. Zardoshti[32], P. Závada[62], B. Zhang[93], C. Zhang[129], L. Zhang[39], M. Zhang[126,6], M. Zhang[27,6], S. Zhang[39], X. Zhang[6], Y. Zhang[118], Y. Zhang[118], Z. Zhang[6], V. Zherebchevskii[140], Y. Zhi[10], D. Zhou[6], Y. Zhou[82], J. Zhu[39], S. Zhu[96,118], Y. Zhu[6], A. Zingaretti[27], S.C. Zugravel[56], N. Zurlo[133,55]

Affiliation Notes

[I] Also at: Max-Planck-Institut fur Physik, Munich, Germany
[II] Also at: Czech Technical University in Prague (CZ)
[III] Also at: Instituto de Fisica da Universidade de Sao Paulo
[IV] Also at: Dipartimento DET del Politecnico di Torino, Turin, Italy
[V] Also at: Department of Applied Physics, Aligarh Muslim University, Aligarh, India
[VI] Also at: Institute of Theoretical Physics, University of Wroclaw, Poland
[VII] Also at: Facultad de Ciencias, Universidad Nacional Autónoma de México, Mexico City, Mexico

Collaboration Institutes

[1] A.I. Alikhanyan National Science Laboratory (Yerevan Physics Institute) Foundation, Yerevan, Armenia
[2] AGH University of Krakow, Cracow, Poland
[3] Bogolyubov Institute for Theoretical Physics, National Academy of Sciences of Ukraine, Kyiv, Ukraine
[4] Bose Institute, Department of Physics and Centre for Astroparticle Physics and Space Science (CAPSS), Kolkata, India
[5] California Polytechnic State University, San Luis Obispo, CA, United States
[6] Central China Normal University, Wuhan, China
[7] Centro de Aplicaciones Tecnológicas y Desarrollo Nuclear (CEADEN), Havana, Cuba
[8] Centro de Investigación y de Estudios Avanzados (CINVESTAV), Mexico City and Mérida, Mexico
[9] Chicago State University, Chicago, IL, United States
[10] China Nuclear Data Center, China Institute of Atomic Energy, Beijing, China
[11] China University of Geosciences, Wuhan, China
[12] Chungbuk National University, Cheongju, Republic of Korea
[13] Comenius University Bratislava, Faculty of Mathematics, Physics and Informatics, Bratislava, Slovak Republic
[14] Creighton University, Omaha, NE, United States
[15] Department of Physics, Aligarh Muslim University, Aligarh, India
[16] Department of Physics, Pusan National University, Pusan, Republic of Korea
[17] Department of Physics, Sejong University, Seoul, Republic of Korea
[18] Department of Physics, University of California, Berkeley, CA, United States
[19] Department of Physics, University of Oslo, Oslo, Norway
[20] Department of Physics and Technology, University of Bergen, Bergen, Norway
[21] Dipartimento di Fisica, Università di Pavia, Pavia, Italy
[22] Dipartimento di Fisica dell'Università and Sezione INFN, Cagliari, Italy
[23] Dipartimento di Fisica dell'Università and Sezione INFN, Trieste, Italy
[24] Dipartimento di Fisica dell'Università and Sezione INFN, Turin, Italy
[25] Dipartimento di Fisica e Astronomia dell'Università and Sezione INFN, Bologna, Italy
[26] Dipartimento di Fisica e Astronomia dell'Università and Sezione INFN, Catania, Italy
[27] Dipartimento di Fisica e Astronomia dell'Università and Sezione INFN, Padova, Italy
[28] Dipartimento di Fisica 'E.R. Caianiello' dell'Università and Gruppo Collegato INFN, Salerno, Italy
[29] Dipartimento DISAT del Politecnico and Sezione INFN, Turin, Italy
[30] Dipartimento di Scienze MIFT, Università di Messina, Messina, Italy
[31] Dipartimento Interateneo di Fisica 'M. Merlin' and Sezione INFN, Bari, Italy
[32] European Organization for Nuclear Research (CERN), Geneva, Switzerland
[33] Faculty of Electrical Engineering, Mechanical Engineering and Naval Architecture, University of Split, Split, Croatia
[34] Faculty of Nuclear Sciences and Physical Engineering, Czech Technical University in Prague, Prague, Czech Republic
[35] Faculty of Physics, Sofia University, Sofia, Bulgaria
[36] Faculty of Science, P.J. Šafárik University, Košice, Slovak Republic
[37] Faculty of Technology, Environmental and Social Sciences, Bergen, Norway
[38] Frankfurt Institute for Advanced Studies, Johann Wolfgang Goethe-Universität Frankfurt, Frankfurt, Germany
[39] Fudan University, Shanghai, China
[40] Gangneung-Wonju National University, Gangneung, Republic of Korea
[41] Gauhati University, Department of Physics, Guwahati, India
[42] Helmholtz-Institut für Strahlen- und Kernphysik, Rheinische Friedrich-Wilhelms-Universität Bonn, Bonn, Germany
[43] Helsinki Institute of Physics (HIP), Helsinki, Finland
[44] High Energy Physics Group, Universidad Autónoma de Puebla, Puebla, Mexico
[45] Horia Hulubei National Institute of Physics and Nuclear Engineering, Bucharest, Romania
[46] HUN-REN Wigner Research Centre, Budapest, Hungary
[47] Indian Institute of Technology Bombay (IIT), Mumbai, India
[48] Indian Institute of Technology Indore, Indore, India
[49] INFN, Laboratori Nazionali di Frascati, Frascati, Italy
[50] INFN, Sezione di Bari, Bari, Italy
[51] INFN, Sezione di Bologna, Bologna, Italy
[52] INFN, Sezione di Cagliari, Cagliari, Italy
[53] INFN, Sezione di Catania, Catania, Italy
[54] INFN, Sezione di Padova, Padova, Italy
[55] INFN, Sezione di Pavia, Pavia, Italy
[56] INFN, Sezione di Torino, Turin, Italy
[57] INFN, Sezione di Trieste, Trieste, Italy
[58] Inha University, Incheon, Republic of Korea
[59] Institute for Gravitational and Subatomic Physics (GRASP), Utrecht University/Nikhef, Utrecht, Netherlands
[60] Institute of Experimental Physics, Slovak Academy of Sciences, Košice, Slovak Republic
[61] Institute of Physics, Homi Bhabha National Institute, Bhubaneswar, India
[62] Institute of Physics of the Czech Academy of Sciences, Prague, Czech Republic
[63] Institute of Space Science (ISS), Bucharest, Romania
[64] Institut für Kernphysik, Johann Wolfgang Goethe-Universität Frankfurt, Frankfurt, Germany
[65] Instituto de Ciencias Nucleares, Universidad Nacional Autónoma de México, Mexico City, Mexico
[66] Instituto de Física, Universidade Federal do Rio Grande do Sul (UFRGS), Porto Alegre, Brazil
[67] Instituto de Física, Universidad Nacional Autónoma de México, Mexico City, Mexico
[68] iThemba LABS, National Research Foundation, Somerset West, South Africa
[69] Jeonbuk National University, Jeonju, Republic of Korea
[70] Korea Institute of Science and Technology Information, Daejeon, Republic of Korea
[71] Laboratoire de Physique Subatomique et de Cosmologie, Université Grenoble-Alpes, CNRS-IN2P3, Grenoble, France
[72] Lawrence Berkeley National Laboratory, Berkeley, CA, United States
[73] Lund University Department of Physics, Division of Particle Physics, Lund, Sweden
[74] Marietta Blau Institute, Vienna, Austria
[75] Nagasaki Institute of Applied Science, Nagasaki, Japan
[76] Nara Women's University (NWU), Nara, Japan
[77] National and Kapodistrian University of Athens, School of Science, Department of Physics, Athens, Greece

[78] National Centre for Nuclear Research, Warsaw, Poland
[79] National Institute of Science Education and Research, Homi Bhabha National Institute, Jatni, India
[80] National Nuclear Research Center, Baku, Azerbaijan
[81] National Research and Innovation Agency - BRIN, Jakarta, Indonesia
[82] Niels Bohr Institute, University of Copenhagen, Copenhagen, Denmark
[83] Nikhef, National Institute for Subatomic Physics, Amsterdam, Netherlands
[84] Nuclear Physics Group, STFC Daresbury Laboratory, Daresbury, United Kingdom
[85] Nuclear Physics Institute of the Czech Academy of Sciences, Husinec-ŘežCzech Republic
[86] Oak Ridge National Laboratory, Oak Ridge, TN, United States
[87] Ohio State University, Columbus, OH, United States
[88] Physics Department, Faculty of Science, University of Zagreb, Zagreb, Croatia
[89] Physics Department, Panjab University, Chandigarh, India
[90] Physics Department, University of Jammu, Jammu, India
[91] Physics Program and International Institute for Sustainability with Knotted Chiral M Matter (WPI-SKCM^2), Hiroshima University, Hiroshima, Japan
[92] Physikalisches Institut, Eberhard-Karls-Universität Tübingen, Tübingen, Germany
[93] Physikalisches Institut, Ruprecht-Karls-Universität Heidelberg, Heidelberg, Germany
[94] Physik Department, Technische Universität München, Munich, Germany
[95] Politecnico di Bari and Sezione INFN, Bari, Italy
[96] Research Division and ExtreMe Matter Institute EMMI, GSI Helmholtzzentrum für Schwerionenforschung GmbH, Darmstadt, Germany
[97] Saga University, Saga, Japan
[98] Saha Institute of Nuclear Physics, Homi Bhabha National Institute, Kolkata, India
[99] School of Physics and Astronomy, University of Birmingham, Birmingham, United Kingdom
[100] Sección Física, Departamento de Ciencias, Pontificia Universidad Católica del Perú, Lima, Peru
[101] SUBATECH, IMT Atlantique, Nantes Université, CNRS-IN2P3, Nantes, France
[102] Sungkyunkwan University, Suwon City, Republic of Korea
[103] Suranaree University of Technology, Nakhon Ratchasima, Thailand
[104] Technical University of Košice, Košice, Slovak Republic
[105] The Henryk Niewodniczanski Institute of Nuclear Physics, Polish Academy of Sciences, Cracow, Poland
[106] The University of Texas at Austin, Austin, TX, United States
[107] Universidad Autónoma de Sinaloa, Culiacán, Mexico
[108] Universidade de São Paulo (USP), São Paulo, Brazil
[109] Universidade Estadual de Campinas (UNICAMP), Campinas, Brazil
[110] Universidade Federal do ABC, Santo Andre, Brazil
[111] Universitatea Nationala de Stiinta si Tehnologie Politehnica Bucuresti, Bucharest, Romania
[112] University of Cape Town, Cape Town, South Africa
[113] University of Derby, Derby, United Kingdom
[114] University of Houston, Houston, TX, United States
[115] University of Jyväskylä, Jyväskylä, Finland
[116] University of Kansas, Lawrence, Kansas, United States
[117] University of Liverpool, Liverpool, United Kingdom
[118] University of Science and Technology of China, Hefei, China
[119] University of Silesia in Katowice, Katowice, Poland
[120] University of South-Eastern Norway, Kongsberg, Norway
[121] University of Tennessee, Knoxville, TN, United States
[122] University of the Witwatersrand, Johannesburg, South Africa
[123] University of Tokyo, Tokyo, Japan
[124] University of Tsukuba, Tsukuba, Japan
[125] Universität Münster, Institut für Kernphysik, Münster, Germany
[126] Université Clermont Auvergne, CNRS/IN2P3, LPC, Clermont-Ferrand, France
[127] Université de Lyon, CNRS/IN2P3, Institut de Physique des 2 Infinis de Lyon, Lyon, France
[128] Université de Strasbourg, CNRS, IPHC UMR 7178, F-67000, Strasbourg, France
[129] Université Paris-Saclay, Centre d'Etudes de Saclay (CEA), IRFU, Département de Physique Nucléaire (DPhN), Saclay, France
[130] Université Paris-Saclay, CNRS/IN2P3, IJCLab, Orsay, France
[131] Università degli Studi di Foggia, Foggia, Italy
[132] Università del Piemonte Orientale, Vercelli, Italy
[133] Università di Brescia, Brescia, Italy
[134] Variable Energy Cyclotron Centre, Homi Bhabha National Institute, Kolkata, India
[135] Warsaw University of Technology, Warsaw, Poland
[136] Wayne State University, Detroit, MI, United States
[137] Yale University, New Haven, CT, United States
[138] Yildiz Technical University, Istanbul, Turkey
[139] Yonsei University, Seoul, Republic of Korea
[140] Affiliated with an institute formerly covered by a cooperation agreement with CERN
[141] Affiliated with an international laboratory covered by a cooperation agreement with CERN

References

[1] S.K. Choi, et al., Belle, Observation of a narrow charmonium-like state in exclusive $B^{\pm} \to K^{\pm}\pi^{+}\pi^{-}J/\psi$ decays, Phys. Rev. Lett. 91 (2003) 262001. hep-ex/0309032, https://doi.org/10.1103/PhysRevLett.91.262001
[2] R. Aaij, et al., LHCb, Observation of J/ψp resonances consistent with pentaquark states in $\Lambda_b^0 \to J/\psi$ K$^-$p decays, Phys. Rev. Lett. 115 (2015) 072001. 1507.03414, https://doi.org/10.1103/PhysRevLett.115.072001
[3] M. Mai, Review of the Λ(1405) a curious case of a strangeness resonance, Eur. Phys. J. Spec. Top. 230 (6) (2021) 1593–1607. 2010.00056, https://doi.org/10.1140/epjs/s11734-021-00144-7
[4] D. Jido, J.A. Oller, E. Oset, A. Ramos, U.G. Meissner, Chiral dynamics of the two Λ(1405) states, Nucl. Phys. A 725 (2003) 181–200. nucl-th/0303062, https://doi.org/10.1016/S0375-9474(03)01598-7
[5] V.K. Magas, E. Oset, A. Ramos, Evidence for the two pole structure of the Λ(1405) resonance, Phys. Rev. Lett. 95 (2005) 052301. hep-ph/0503043, https://doi.org/10.1103/PhysRevLett.95.052301
[6] J.A. Oller, U.G. Meissner, Chiral dynamics in the presence of bound states: kaon-nucleon interactions revisited, Phys. Lett. B 500 (2001) 263–272. hep-ph/0011146, https://doi.org/10.1016/S0370-2693(01)00078-8
[7] I. Zychor, et al., Shape of the Λ(1405) hyperon measured through its $\Sigma^0\,\pi^0$ decay, Phys. Lett. B 660 (2008) 167–171. 0705.1039, https://doi.org/10.1016/j.physletb.2008.01.002
[8] G. Agakishiev, et al., HADES, Baryonic resonances close to the $\overline{K}N$ threshold: the case of Λ(1405) in pp collisions, Phys. Rev. C 87 (2013) 025201. https://link.aps.org/doi/10.1103/PhysRevC.87.025201. https://doi.org/10.1103/PhysRevC.87.025201
[9] K. Moriya, et al., CLAS, Spin and parity measurement of the Λ(1405) baryon, Phys. Rev. Lett. 112 (2014) 082004. https://link.aps.org/doi/10.1103/PhysRevLett.112.082004. https://doi.org/10.1103/PhysRevLett.112.082004
[10] A. Ramos, E. Oset, C. Bennhold, On the spin, parity and nature of the Ξ(1620) resonance, Phys. Rev. Lett. 89 (2002) 252001. nucl-th/0204044, https://doi.org/10.1103/PhysRevLett.89.252001
[11] A. Feijoo, V. Valcarce Cadenas, V.K. Magas, The Ξ(1620) and Ξ(1690) molecular states from $S = -2$ meson-baryon interaction up to next-to-leading order, Phys. Lett. B 841 (2023) 137927. [Erratum: Phys.Lett.B 853, 138660 (2024)]. 2303.01323, https://doi.org/10.1016/j.physletb.2023.137927
[12] M. Sumihama, et al., Belle, Observation of $\Xi(1620)^0$ and evidence for $\Xi(1690)^0$ in $\Xi_c^+ \to \Xi^-\pi^+\pi^+$ decays, Phys. Rev. Lett. 122 (7) (2019) 072501. 1810.06181, https://doi.org/10.1103/PhysRevLett.122.072501
[13] V.M. Sarti, A. Feijoo, I. Vidaña, A. Ramos, F. Giacosa, T. Hyodo, Y. Kamiya, Constraining the low-energy S = −2 meson-baryon interaction with two-particle correlations, Phys. Rev. D 110 (1) (2024) L011505. 2309.08756, https://doi.org/10.1103/PhysRevD.110.L011505
[14] A. Feijoo, V.M. Sarti, J. Nieves, A. Ramos, I. Vidaña, Bridging correlation and spectroscopy measurements to access the hadron interaction behind molecular states: the case of the Ξ(1620) and Ξ(1690) in the K-Λ system, Phys. Rev. D 111 (1) (2025) 014022. 2411.10245, https://doi.org/10.1103/PhysRevD.111.014022
[15] R. Aaij, et al., LHCb, Evidence of a $J/\psi\Lambda$ structure and observation of excited Ξ^- states in the $\Xi_b^- \to J/\psi\Lambda K^-$ decay, Sci. Bull. 66 (2021) 1278–1287. 2012.10380, https://doi.org/10.1016/j.scib.2021.02.030
[16] S. Weinberg, Phenomenological Lagrangians, Physica A 96 (1–2) (1979) 327–340. https://doi.org/10.1016/0378-4371(79)90223-1

[17] J. Gasser, H. Leutwyler, Chiral perturbation theory to one loop, Ann. Phys. 158 (1984) 142. https://doi.org/10.1016/0003-4916(84)90242-2

[18] C. Garcia-Recio, M.F.M. Lutz, J. Nieves, Quark mass dependence of s-wave baryon resonances, Phys. Lett. B 582 (2004) 49–54. nucl-th/0305100, https://doi.org/10.1016/j.physletb.2003.11.073

[19] A. Pich, Effective field theory: course, in: Les Houches Summer School in Theoretical Physics, Session 68: Probing the Standard Model of Particle Interactions, 1998, pp. 949–1049. hep-ph/9806303

[20] A. Feijoo, V.K. Magas, A. Ramos, The $\overline{K}N \to K\Xi$ reaction in coupled channel chiral models up to next-to-leading order, Phys. Rev. C 92 (1) (2015) 015206. 1502.07956, https://doi.org/10.1103/PhysRevC.92.015206

[21] S. Acharya, et al., ALICE, Unveiling the strong interaction among hadrons at the LHC, Nature 588 (7837) (2020) 232–238. 2005.11495, https://doi.org/10.1038/s41586-020-3001-6

[22] L. Fabbietti, V.M. Sarti, O.V. Doce, Study of the strong interaction among hadrons with correlations at the LHC, Ann. Rev. Nucl. Part. Sci. 71 (2021) 377–402. 2012.09806, https://doi.org/10.1146/annurev-nucl-102419-034438

[23] S. Acharya, et al., ALICE, Accessing the strong interaction between Λ baryons and charged kaons with the femtoscopy technique at the LHC, Phys. Lett. B 845 (2023) 138145. 2305.19093, https://doi.org/10.1016/j.physletb.2023.138145

[24] S. Acharya, et al., ALICE, ΛK femtoscopy in Pb–Pb collisions at $\sqrt{s_{NN}} = 2.76$ TeV, Phys. Rev. C 103 (5) (2021) 055201. 2005.11124, https://doi.org/10.1103/PhysRevC.103.055201

[25] W.E. Humphrey, R.R. Ross, Low-energy interactions of K^- mesons in hydrogen, Phys. Rev. 127 (1962) 1305–1323. https://doi.org/10.1103/PhysRev.127.1305

[26] M.B. Watson, M. Ferro-Luzzi, R.D. Tripp, Analysis of Y_0^* (1520) and determination of the Σ parity, Phys. Rev. 131 (1963) 2248–2281. https://doi.org/10.1103/PhysRev.131.2248

[27] T.S. Mast, M. Alston-Garnjost, R.O. Bangerter, A.S. Barbaro-Galtieri, F.T. Solmitz, R.D. Tripp, Elastic, charge exchange, and total K- p cross sections in the momentum range 220 MeV/c to 470 MeV/c, Phys. Rev. D14 (1976) 13. https://doi.org/10.1103/PhysRevD.14.13

[28] R.J. Nowak, et al., Charged Σ hyperon production by K^- meson interactions at rest, Nucl. Phys. B139 (1978) 61–71. https://doi.org/10.1016/0550-3213(78)90179-7

[29] J. Ciborowski, et al., Kaon scattering and charged sigma hyperon production in K^-p interactions below 300 MeV/c, J. Phys. G8 (1982) 13–32. https://doi.org/10.1088/0305-4616/8/1/005

[30] K. Piscicchia, et al., First simultaneous $K^-p \to \Sigma^0\pi^0, \Lambda\pi^0$ cross section measurements at 98 MeV/c, Phys. Rev. C 108 (5) (2023) 055201. 2210.10342, https://doi.org/10.1103/PhysRevC.108.055201

[31] M. Bazzi, et al., SIDDHARTA, A new measurement of kaonic hydrogen X-rays, Phys. Lett. B 704 (2011) 113–117. 1105.3090, https://doi.org/10.1016/j.physletb.2011.09.011

[32] S. Acharya, et al., ALICE, Scattering studies with low-energy kaon-proton femtoscopy in proton–proton collisions at the LHC, Phys. Rev. Lett. 124 (2020) 092301. 1905.13470, https://doi.org/10.1103/PhysRevLett.124.092301

[33] S. Acharya, et al., ALICE, Constraining the $\overline{K}N$ coupled channel dynamics using femtoscopic correlations at the LHC, Eur. Phys. J. C 83 (4) (2023) 340. 2205.15176, https://doi.org/10.1140/epjc/s10052-023-11476-0

[34] S. Acharya, et al., ALICE, Kaon–proton strong interaction at low relative momentum via femtoscopy in Pb–Pb collisions at the LHC, Phys. Lett. B 822 (2021) 136708. 2105.05683, https://doi.org/10.1016/j.physletb.2021.136708

[35] A. Starostin, et al., Crystal Ball, Measurement of K^- p $\to \eta\Lambda$ near threshold, Phys. Rev. C 64 (2001) 055205. https://doi.org/10.1103/PhysRevC.64.055205

[36] D.F. Baxter, et al., A study of neutral final states in K^-p interactions in the range from 690 to 934 MeV/c, Nucl. Phys. B 67 (1973) 125–156. https://doi.org/10.1016/0550-3213(73)90322-2

[37] M. Jones, R. Levi Setti, D. Merrill, R.D. Tripp, K^-p charge exchange and hyperon production cross sections from 860 MeV/c to 1000 MeV/c, Nucl. Phys. B 90 (1975) 349–383. https://doi.org/10.1016/0550-3213(75)90652-5

[38] A. Berthon, et al., Cross-sections for quasi-two-body reactions in K^-p interactions between 1263 and 1843 MeV/c, Nuovo Cim. A 21 (1974) 146–167. https://doi.org/10.1007/BF02731189

[39] J.K. Kim, Low energy K^-p interaction and interpretation of the 1405-MeV Y_0^* resonance as $\overline{K}N$ bound state, Phys. Rev. Lett. 14 (1965) 29. https://doi.org/10.1103/PhysRevLett.14.29

[40] R.O. Bangerter, M. Alston-Garnjost, A. Barbaro-Galtieri, T.S. Mast, F.T. Solmitz, R.D. Tripp, Reactions K^- p $\to \Sigma^-\pi^+$ and K^- p $\to \Sigma^+\pi^-$ in the momentum range from 220 MeV/c to 470 MeV/c, Phys. Rev. D 23 (1981) 1484. https://doi.org/10.1103/PhysRevD.23.1484

[41] G. Burgun, et al., Resonance formation in the reactions $K^-p \to K^-\Xi^-$ and $K^-p \to K^0\Xi^0$ in the mass region from 1915 to 2168 MeV, Nucl. Phys. B 8 (1968) 447–459. https://doi.org/10.1016/0550-3213(68)90256-3

[42] J.R. Carlson, H.F. Davis, D.E. Jauch, N.D. Sossong, R. Ellsworth, Measurement of neutral cascade production from negative-kaon-hydrogen at 1.8 GeV/c, $K^-p \to K^0\Xi^0$, Phys. Rev. D 7 (1973) 2533–2537. https://doi.org/10.1103/PhysRevD.7.2533

[43] P.M. Dauber, J.P. Berge, J.R. Hubbard, D.W. Merrill, R.A. Muller, Production and decay of cascade hyperons, Phys. Rev. 179 (1969) 1262–1285. https://doi.org/10.1103/PhysRev.179.1262

[44] M. Haque, et al., Birmingham-Glasgow-London(I.C.)-Oxford-Rutherford, Reactions $K^-p \to$ hyperon + meson at 3.5 GeV/c, Phys. Rev. 152 (1966) 1148–1161. https://doi.org/10.1103/PhysRev.152.1148

[45] G.W. London, R.R. Rau, N.P. Samios, S.S. Yamamoto, M. Goldberg, S. Lichtman, M. Prime, J. Leitner, K^-p interaction at 2.24 BeV/c, Phys. Rev. 143 (1966) 1034–1091. https://doi.org/10.1103/PhysRev.143.1034

[46] T.G. Trippe, P.E. Schlein, Partial wave analysis of $K^-p \to \Xi K^+$ at 2 GeV, Phys. Rev. 158 (5) (1967) 1334–1337. https://doi.org/10.1103/PhysRev.158.1334

[47] A. Ramos, A. Feijoo, V.K. Magas, The chiral S = −1 meson–baryon interaction with new constraints on the NLO contributions, Nucl. Phys. A 954 (2016) 58–74. 1605.03767, https://doi.org/10.1016/j.nuclphysa.2016.05.006

[48] H. Kamano, S.X. Nakamura, T.-S.H. Lee, T. Sato, Dynamical coupled channels model of K^-p reactions: determination of partial wave amplitudes, Phys. Rev. C 90 (6) (2014) 065204. 1407.6839, https://doi.org/10.1103/PhysRevC.90.065204

[49] H. Kamano, S.X. Nakamura, T.-S.H. Lee, T. Sato, Dynamical coupled-channels model of K^-p reactions. II. Extraction of Λ^* and Σ^* hyperon resonances, Phys. Rev. C 92 (2) (2015) 025205. [Erratum: Phys.Rev.C 95, 049903 (2017)]. 1506.01768, https://doi.org/10.1103/PhysRevC.92.025205

[50] A. Feijoo, V. Magas, A. Ramos, S = −1 meson-baryon interaction and the role of isospin filtering processes, Phys. Rev. C 99 (3) (2019) 035211. 1810.07600, https://doi.org/10.1103/PhysRevC.99.035211

[51] M. Döring, J. Haidenbauer, M. Mai, T. Sato, Dynamical coupled-channel models for hadron dynamics (2025). arXiv:2505.02745

[52] P. Encarnación, A. Feijoo, V.M. Sarti, A. Ramos, Femtoscopic study of the S = −1 meson-baryon interaction: K-p, π-Λ, and K + Ξ- correlations, Phys. Rev. D 111 (11) (2025) 114013. 2412.20880, https://doi.org/10.1103/3ycr-vzmd

[53] K. Aamodt, et al., ALICE, The ALICE experiment at the CERN LHC, J. Instrum. 3 (2008) S08002. https://doi.org/10.1088/1748-0221/3/08/S08002

[54] E. Abbas, et al., ALICE, Performance of the ALICE VZERO system, J. Instrum. 8 (2013) P10016. 1306.3130, https://doi.org/10.1088/1748-0221/8/10/p10016

[55] K. Aamodt, et al., ALICE, Alignment of the ALICE inner tracking system with cosmic-ray tracks, JINST 5 (2010) P03003. 1001.0502, https://doi.org/10.1088/1748-0221/5/03/P03003

[56] B. Abelev, et al., ALICE, Performance of the ALICE experiment at the CERN LHC, Int. J. Mod. Phys. A29 (2014) 1430044. 1402.4476, https://doi.org/10.1142/S0217751X14300440

[57] J. Adam, et al., ALICE, Enhanced production of multi-strange hadrons in high-multiplicity proton-proton collisions, Nat. Phys. 13 (2017) 535–539. 1606.07424, https://doi.org/10.1038/nphys4111

[58] J. Alme, Y. Andres, H. Appelshäuser, S. Bablok, N. Bialas, et al., The ALICE TPC, a large 3-dimensional tracking device with fast readout for ultra-high multiplicity events, Nucl. Instrum. Meth. A622 (2010) 316–367. 1001.1950, https://doi.org/10.1016/j.nima.2010.04.042

[59] A. Akindinov, et al., Performance of the ALICE time-of-flight detector at the LHC, Eur. Phys. J. Plus 128 (2013) 44. https://doi.org/10.1140/epjp/i2013-13044-x

[60] S. Acharya, et al., ALICE, Study of the p–p–K^+ and p–p–K^- dynamics using the femtoscopy technique, Eur. Phys. J. A 59 (12) (2023) 298. 2303.13448, https://doi.org/10.1140/epja/s10050-023-01139-9

[61] S. Acharya, et al., ALICE, Studying the interaction between charm and light-flavor mesons, Phys. Rev. D 110 (3) (2024) 032004 . 2401.13541, https://doi.org/10.1103/PhysRevD.110.032004

[62] S. Acharya, et al., ALICE, Investigating the p–$\pi^\pm$ and p–p–$\pi^\pm$ dynamics with femtoscopy in pp collisions at $\sqrt{s} = \mathbf{13}$ TeV, Eur. Phys. J. A 61 (8) (2025) 194. 2502.20200, https://doi.org/10.1140/epja/s10050-025-01615-4

[63] S. Acharya, et al., ALICE, Exploring the strong interaction of three-body systems at the LHC, Phys. Rev. X 14 (3) (2024) 031051. 2308.16120, https://doi.org/10.1103/PhysRevX.14.031051

[64] S. Acharya, et al., ALICE, p-p, p-Λ and Λ-Λ correlations studied via femtoscopy in pp reactions at $\sqrt{s} = 7$ TeV, Phys. Rev. C99 (2019) 024001. 1805.12455, https://doi.org/10.1103/PhysRevC.99.024001

[65] S. Navas, et al., Particle Data Group, Review of particle physics, Phys. Rev. D 110 (3) (2024) 030001. https://doi.org/10.1103/PhysRevD.110.030001

[66] S. Acharya, et al., ALICE, Probing strangeness hadronization with event-by-event production of multistrange hadrons, Phys. Rev. Lett. 134 (2) (2025) 022303. 2405.19890, https://doi.org/10.1103/PhysRevLett.134.022303

[67] S. Acharya, et al., ALICE, First study of the two-body scattering involving charm hadrons, Phys. Rev. D 106 (5) (2022) 052010. 2201.05352, https://doi.org/10.1103/PhysRevD.106.052010

[68] R. Brun, F. Bruyant, F. Carminati, S. Giani, M. Maire, A. McPherson, G. Patrick, L. Urban, GEANT detector description and simulation tool, CERN-W5013 (1994). https://doi.org/10.17181/CERN.MUHF.DMJ1

[69] S. Acharya, et al., ALICE, Common femtoscopic hadron-emission source in pp collisions at the LHC (2023). arXiv:2311.14527

[70] D.L. Mihaylov, V. Mantovani Sarti, O.W. Arnold, L. Fabbietti, B. Hohlweger, A.M. Mathis, A femtoscopic correlation analysis tool using the Schrödinger equation (CATS), Eur. Phys. J. C 78 (2018) 394. 1802.08481, https://doi.org/10.1140/epjc/s10052-018-5859-0

[71] S. Acharya, et al., ALICE, Study of the Λ-Λ interaction with femtoscopy correlations in pp and p–Pb collisions at the LHC, Phys. Lett. B 797 (2019) 134822. 1905.07209, https://doi.org/10.1016/j.physletb.2019.134822

[72] B.B. Abelev, et al., ALICE, Production of $\Sigma(1385)^\pm$ and $\Xi(1530)^0$ in proton-proton collisions at $\sqrt{s} = 7$ TeV, Eur. Phys. J. C 75 (1) (2015) 1. 1406.3206, https://doi.org/10.1140/epjc/s10052-014-3191-x

[73] R. Lednický, Finite-size effects on two-particle production in continuous and discrete spectrum, Phys. Part. Nucl. 40 (2009) 307–352. nucl-th/0501065, https://doi.org/10.1134/S1063779609030034

[74] M. Albaladejo, A. Garcia-Lorenzo, J. Nieves, Femtoscopy correlation functions and hadron-hadron scattering amplitudes in presence of Coulomb potential, PTEP 2025 (2025) 09. 2503.18710, https://doi.org/10.1093/ptep/ptaf095

[75] M. Albaladejo, A. Feijoo, J. Nieves, E. Oset, I. Vidaña, Femtoscopy correlation functions and mass distributions from production experiments, Phys. Rev. D 110 (11) (2024) 114052. 2410.08880, https://doi.org/10.1103/PhysRevD.110.114052

[76] J.M. Torres-Rincon, A. Ramos, J. Rufí, Two-body femtoscopy approach to the proton-deuteron correlation function, Phys. Rev. C 111 (4) (2025) 044906. 2410.23853, https://doi.org/10.1103/PhysRevC.111.044906
[77] A. Feijoo, M. Korwieser, L. Fabbietti, Relevance of the coupled channels in the ϕp and ρ^0p correlation functions, Phys. Rev. D 111 (1) (2025) 014009. 2407.01128, https://doi.org/10.1103/PhysRevD.111.014009
[78] M.A. Lisa, S. Pratt, R. Soltz, U. Wiedemann, Femtoscopy in relativistic heavy ion collisions, Ann. Rev. Nucl. Part. Sci. 55 (2005) 357–402. nucl-ex/0505014, https://doi.org/10.1146/annurev.nucl.55.090704.151533
[79] S.E. Koonin, Proton pictures of high-energy nuclear collisions, Phys. Lett. B 70 (1977) 43–47. https://doi.org/10.1016/0370-2693(77)90340-9
[80] S. Acharya, et al., ALICE, Search for a common baryon source in high-multiplicity pp collisions at the LHC, Phys. Lett. B 811 (2020) 135849. 2004.08018, https://doi.org/10.1016/j.physletb.2020.135849
[81] S. Acharya, et al., ALICE, Corrigendum to: search for a common baryon source in high-multiplicity pp collisions at the LHC, Phys. Lett. B 861 (2025) 139233. https://doi.org/10.1016/j.physletb.2024.139233
[82] S. Acharya, et al., ALICE, Experimental evidence for an attractive p-ϕ interaction, Phys. Rev. Lett. 127 (17) (2021) 172301. 2105.05578, https://doi.org/10.1103/PhysRevLett.127.172301
[83] J. Adam, et al., ALICE, Insight into particle production mechanisms via angular correlations of identified particles in pp collisions at $\sqrt{s} = 7$ TeV, Eur. Phys. J. C77 (8) (2017) 569. [Erratum: *Eur. Phys. J. C* 79 no.12 (2019)]. 1612.08975, https://doi.org/10.1140/epjc/s10052-019-7398-8
[84] S. Acharya, et al., ALICE, Investigating the role of strangeness in baryon–antibaryon annihilation at the LHC, Phys. Lett. B 829 (2022) 137060. 2105.05190, https://doi.org/10.1016/j.physletb.2022.137060
[85] T. Sjöstrand, S. Ask, J.R. Christiansen, R. Corke, N. Desai, P. Ilten, S. Mrenna, S. Prestel, C.O. Rasmussen, P.Z. Skands, An introduction to PYTHIA 8.2, Comput. Phys. Commun. 191 (2015) 159–177. 1410.3012, https://doi.org/https://doi.org/10.1016/j.cpc.2015.01.024
[86] P. Skands, S. Carrazza, J. Rojo, Tuning PYTHIA 8.1: the monash 2013 tune, Eur. Phys. J. C 74 (8) (2014) 3024. 1404.5630, https://doi.org/10.1140/epjc/s10052-014-3024-y
[87] S. Acharya, et al., ALICE, Studying strangeness and baryon production mechanisms through angular correlations between charged Ξ baryons and identified hadrons in pp collisions at $\sqrt{s} = 13$ TeV, JHEP 09 (2024) 102. 2308.16706, https://doi.org/10.1007/JHEP09(2024)102
[88] C. Bierlich, S. Chakraborty, G. Gustafson, L. Lönnblad, Strangeness enhancement across collision systems without a plasma, Phys. Lett. B 835 (2022) 137571. 2205.11170, https://doi.org/10.1016/j.physletb.2022.137571
[89] M. Matveev, A.V. Sarantsev, V.A. Nikonov, A.V. Anisovich, U. Thoma, E. Klempt, Hyperon I: partial-wave amplitudes for K^-p scattering, Eur. Phys. J. A 55 (10) (2019) 179. 1907.03645, https://doi.org/10.1140/epja/i2019-12878-y
[90] A.V. Sarantsev, M. Matveev, V.A. Nikonov, A.V. Anisovich, U. Thoma, E. Klempt, Hyperon II: properties of excited hyperons, Eur. Phys. J. A 55 (10) (2019) 180. 1907.13387, https://doi.org/10.1140/epja/i2019-12880-5
[91] A.V. Anisovich, A.V. Sarantsev, V.A. Nikonov, V. Burkert, R.A. Schumacher, U. Thoma, E. Klempt, Hyperon III: $K^-p - \pi\Sigma$ coupled-channel dynamics in the $\Lambda(1405)$ mass region, Eur. Phys. J. A 56 (5) (2020) 139. https://doi.org/10.1140/epja/s10050-020-00142-8
[92] H. Zhang, J. Tulpan, M. Shrestha, D.M. Manley, Multichannel parametrization of $\bar{K}N$ scattering amplitudes and extraction of resonance parameters, Phys. Rev. C 88 (3) (2013) 035205. 1305.4575, https://doi.org/10.1103/PhysRevC.88.035205
[93] W.H. Press, S.A. Teukolsky, W.T. Vetterling, B.P. Flannery, Numerical Recipes 3rd Edition: The Art of Scientific Computing, Cambridge University Press, pp. 809–810.
[94] J. Bartsch, et al., Aachen-Berlin-CERN-London-Vienna, Evidence for a new Ξ resonance at 2500 MeV in 10 GeV/c K^-p interactions, Phys. Lett. B 28 (1969) 439–442. https://doi.org/10.1016/0370-2693(69)90346-3
[95] J. Alitti, et al., Strangeness S = −2 baryon resonance, Phys. Rev. Lett. 22 (1969) 79–82. https://doi.org/10.1103/PhysRevLett.22.79
[96] C.M. Jenkins, et al., Existence of Ξ resonances above 2 GeV, Phys. Rev. Lett. 51 (1983) 951–954. https://doi.org/10.1103/PhysRevLett.51.951